

GAMMA-RAY LOUDNESS, SYNCHROTRON PEAK FREQUENCY, AND PARSEC-SCALE PROPERTIES OF BLAZARS DETECTED BY THE *FERMI* LARGE AREA TELESCOPE

J. D. Linford, G. B. Taylor, and F. K. Schinzel

University of New Mexico

Department of Physics and Astronomy, MSC07 4220, Albuquerque, NM 87131-0001, USA

jlinford@unm.edu

ABSTRACT

The parsec-scale radio properties of 232 active galactic nuclei (AGNs), most of which are blazars, detected by the Large Area Telescope (LAT) on board the *Fermi Gamma-ray Space Telescope* have been observed contemporaneously by the Very Long Baseline Array (VLBA) at 5 GHz. Data from both the first 11 months (1FGL) and the first 2 years (2FGL) of the *Fermi* mission were used to investigate these sources' γ -ray properties. We use the ratio of the γ -ray to radio luminosity as a measure of γ -ray loudness. We investigate the relationship of several radio properties to γ -ray loudness and to the synchrotron peak frequency. There is a tentative correlation between γ -ray loudness and synchrotron peak frequency for BL Lac objects in both 1FGL and 2FGL, and for flat-spectrum radio quasars (FSRQs) in 2FGL. We find that the apparent opening angle tentatively correlates with γ -ray loudness for FSRQs, but only when we use the 2FGL data. We also find that the total VLBA flux density correlates with the synchrotron peak frequency for BL Lac objects and FSRQs. The core brightness temperature also correlates with synchrotron peak frequency, but only for the BL Lac objects. The low-synchrotron peaked (LSP) BL Lac object sample shows indications of contamination by FSRQs which happen to have undetectable emission lines. There is evidence that the LSP BL Lac objects are more strongly beamed than the rest of the BL Lac object population.

Subject headings: BL Lacertae objects: general - galaxies: active - galaxies: jets - galaxies: nuclei - gamma-rays: galaxies - quasars: general - radio continuum: galaxies

1. Introduction

The Large Area Telescope (LAT; Atwood et al. 2009) on board the *Fermi Gamma-ray Space Telescope* is a wide-field telescope covering the energy range from about 20 MeV to more than 300 GeV. It has been scanning the entire γ -ray sky once every three hours since July of 2008, with breaks for flares and other targets of opportunity. The majority of the sources (685 of 1451) in the *Fermi* LAT First Source Catalog (1FGL; Abdo et al. 2010a) have been identified with known radio blazars. These blazars typically are active galactic nuclei (AGNs) with strong, compact radio sources which exhibit flat radio spectra, rapid variability, compact cores with one-sided parsec-scale jets, and superluminal motion in the jets (Marscher 2006). This trend continues in the newly released *Fermi* LAT Second Source Catalog (2FGL; Nolan et al. 2011), compiled using the first two years of LAT data.

We previously presented findings on the relationships between the LAT-detected and non-LAT-detected populations of blazars (Linford et al. 2011; Linford et al. 2012). Like other studies, we found a strong correlation between LAT flux and total VLBA radio flux density. We also found that the LAT and non-LAT BL Lac objects appeared to be similar in many respects, while the LAT flat-spectrum radio quasars (FSRQs) were extreme sources when compared to their non-LAT counterparts. Polarized emission at the base of the jets was also reported to be significantly more frequent in LAT blazars than in non-LAT blazars.

A major program to monitor the parsec-scale radio (15 GHz) properties of these γ -ray emitting blazars is the Monitoring Of Jets in AGN with VLBA Experiments (MOJAVE; Lister et al. 2009a; Homan et al. 2009). The MOJAVE and *Fermi* LAT collaborations recently published a paper detailing their investigations of parsec-scale properties of the γ -ray emitting blazars in their sample (Lister et al. 2011). They studied the relationships between radio properties and the γ -ray loudness (G_r ; the ratio of γ -ray-to-radio luminosity) and synchrotron peak frequency (ν_{peak}^S ; the frequency where the synchrotron emission is at maximum). They reported significant differences in the G_r distributions between the BL Lac objects and FSRQs. For their BL Lac objects, they reported strong correlations for G_r - ν_{peak}^S and G_r - γ -ray photon spectral index. They also reported a non-linear correlation between apparent jet opening angle and G_r for their entire sample. Their high-synchrotron peaked ($\nu_{peak}^S > 10^{15}$) BL Lac objects tended to have lower core brightness temperatures, linear core polarization, and variability than the rest of their BL Lac object population.

Here, we have analyzed our recent VLBA 5 GHz data, taken contemporaneously with LAT observations (Linford et al. 2012), to see if we could reproduce the findings of Lister et al. (2011). Our sample was slightly larger than the one presented in Lister et al. (2011), with 232 sources in our sample compared to 173 in theirs. We had a larger fraction of BL Lac objects in our sample, and we also had more non-blazar AGNs (radio galaxies, AGN

of unknown type, and one starburst galaxy). The objects in our sample spanned a larger range of radio flux densities, as the MOJAVE sample is targeting the brightest AGN and our sample is radio flux limited. We only had single observations on our sources, as we are not a monitoring program. This leads to some difficulties in comparing with the MOJAVE sample, especially in terms of apparent jet opening angle.

Another area that has garnered renewed interest in the *Fermi*-LAT era is the unification system for AGN (e.g., Urry & Padovani 1995). Several groups (e.g., Nieppola et al. 2008, Ghisellini & Tavecchio 2008, Meyer et al. 2011, and Giommi et al. 2012b) have been investigating the “blazar sequence” (Fossati et al. 1998, Ghisellini et al. 1998), the relationship between blazar luminosity and synchrotron peak frequency. There have been hints (Vermeulen et al. 1995, Ghisellini et al. 2009, Giommi et al. 2012a, Meyer et al. 2011) that the population of BL Lac objects with low (below 10^{14} Hz) synchrotron peak frequencies might actually contain some misidentified FSRQs which happen to have strong emission from their jets overpowering their emission lines. We investigated the possibility for this kind of “contamination” in our sample and present our findings here.

In Section 2 we define our sample. In Section 3 we discuss how we determined the γ -ray loudness and synchrotron peak frequency for our sources. In Section 4 we present our results and discuss their implications. In Section 5, we present evidence that our LSP BL Lac object sample may have some FSRQs hiding in it. Throughout this paper we assume Λ CDM cosmology with $H_0 = 71 \text{ km s}^{-1} \text{ Mpc}^{-1}$, $\Omega_m = 0.27$, and $\Omega_\Lambda = 0.73$ (e.g., Hinshaw et al. 2009).

2. Sample Definition

The radio observations of our 232 sources were done with the Very Long Baseline Array (VLBA) at 5 GHz between 2009 November and 2010 July. This is the sample described in more detail in Linford et al. (2012). We included 90 sources that were follow-up observations of sources in the VLBA Imaging and Polarimetry Survey (VIPS; Helmboldt et al. 2007) as well as new 5 GHz observations of 7 MOJAVE sources. The VIPS follow-up (or “VIPS+”) sample can be thought of as radio-selected as the sources were originally selected and observed prior to the launch of *Fermi*. The remaining 135 sources (“VIPS++”) can be thought of as γ -ray-selected as they were specifically targeted due to their presence in 1FGL. Where possible, we used the optical classifications from the LAT Second Catalog of AGN (2LAC; Ackermann et al. 2011). If a source was not in 2LAC, we used the classification from the LAT First Catalog of AGN (1LAC; Abdo et al. 2010b). In general, a source is classified as a BL Lac object if its strongest optical emission line has an equivalent width (EW) less than

5 Å and the optical spectrum shows a CA II H/K break ratio of less than 0.4. An object is classified as a FSRQ if it has a flat radio spectrum and its optical spectrum is dominated by broad ($EW > 5$ Å) emission lines. While we do not suspect widespread misclassification (such a problem would have a serious negative impact on our results and the results of every other study based on LAT data), we do present evidence that some objects classified as BL Lac objects may actually be FSRQs (see Section 5). We should note that many sources classified in 1LAC as “non-blazar AGN” and “AGN of unknown type” were reclassified as BL Lac objects or FSRQs in 2LAC. Therefore, the optical classifications for some of our objects are different than in Linford et al. (2012). Our 1FGL sample contained 105 BL Lac objects, 114 FSRQs, and 13 other types of AGNs (radio galaxies, AGNs of unknown type, and 1 starburst galaxy). Wherever possible, we used the 1LAC and 2LAC redshifts. If a source did not have a redshift listed in 1LAC or 2LAC, we searched the NASA/IPAC Extragalactic Database (NED).

With the release of 2FGL and 2LAC, we also had newer data on several of our sources. Unfortunately, not all of the sources in 1LAC were present in 2LAC, and some of our sources were among those dropped. Our 2FGL sample contained 215 objects; 98 BL Lac objects, 108 FSRQs, and 9 AGN/Other. Several 1FGL sources were dropped in 2FGL. The 2FGL was based on 24 months of observing and some sources that were in a high-activity state (i.e., flaring) during the 1FGL period later decreased in brightness below the LAT threshold and their average flux failed to meet the criteria for inclusion in 2FGL. For further discussion of the 1FGL-2FGL source comparisons, see Nolan et al. (2012).

While our sample is not statistically complete (i.e., it does not contain all northern hemisphere sources with a flux density greater than 30 mJy), it is representative of the LAT-detected blazar population. It covers a wide range in flux density but is more biased towards relatively weak ($S < 1$ Jy) radio sources compared to the sample in Lister et al. (2011). Because of this, we can expect to have fewer sources with low (< 100) γ -ray loudness (see Section 3.1) than in the sample presented in Lister et al. (2011). Also, we are likely to have more BL Lac objects in our sample than other studies with a higher flux density threshold. Our sample also covers a wide range of luminosities, synchrotron peak frequencies, and γ -ray loudness. As Lister et al. (2011) discussed, representative samples are appropriate for statistical investigations and selection biases are not expected to have significant impacts on our results. Obviously, the statistics of any study would be improved if a truly complete sample (i.e., simultaneous monitoring of all LAT-detected blazars observable by the VLBA) existed. However, such a sample would require a prohibitive amount of VLBA observing time (in fact, it would probably have to be the only project observed for an entire year) to be practical. Furthermore, a discussion of the biases introduced by our selection criteria would be, at best, speculation at this time as the complete parent sample of LAT sources

has yet to be fully characterized. The 2FGL catalog contains 577 sources with no known radio or optical association, which means we do not know what 31% of the 2FGL sources are. Also, of the 1121 entries in 2LAC, 270 are “AGN of unknown type”, 11 are simply described as “non-blazar AGN”, and 6 are listed as “unidentified”.

The sample presented in Lister et al. (2011) is the combination of 2 statistically complete samples: a radio-selected sample and a γ -ray selected sample. While the two samples on their own are complete, the combination is again representative. Their sample contains more objects with high (> 1 Jy) flux density than ours, but they did not have as many sources with low (< 500 mJy) flux density. Our sample contains more sources (232 versus 173), and in particular more BL Lac objects (105 versus 45), but our sample has fewer FSRQs (114 versus 123).

3. Gamma-ray Loudness and Synchrotron Peak Frequency

3.1. Gamma-ray Loudness

We adopted the definition of Lister et al. (2011) for “ γ -ray loudness” as the ratio of the γ -ray luminosity to the radio luminosity. Unlike Lister et al. (2011), we did not have multiple observations on our sources from which to determine a median radio luminosity. Instead, we only used a single observation to calculate a luminosity. Due to the variable nature of these blazars, this may not be the best representation of the sources’ actual average luminosity. For the γ -ray luminosity, we used the average fluxes reported in the 1FGL and the 2FGL. The LAT measures γ -ray flux continuously from 20 MeV to over 300 GeV. For publication (e.g., in 1FGL and 2FGL) the measurements are later grouped into energy bands in order to provide spectral information. To obtain total γ -ray fluxes, we combined the fluxes from 3 bands where the LAT has the highest sensitivity: 100-300 MeV, 300 MeV - 1 GeV, and 1-100 GeV. The fluxes were added and uncertainties were added in quadrature. However, some sources had only upper limits to their fluxes in certain bands. If a source’s reported fluxes in one of the bands were upper limits, we use as the uncertainty half the reported flux in that band because the upper limits are given as 2-sigma results (Abdo et al. 2010a).

To calculate the γ -ray luminosities, we used the same process as Lister et al. (2011). We calculated the luminosities using data from both 1FGL/1LAC and 2FGL/2LAC, when available. We started with converting energy fluxes using the equation

$$S_{0.1} = \frac{(\Gamma_0 - 1)C_1 E_1 F_{0.1}}{(\Gamma_0 - 2)} \left[1 - \frac{E_1}{E_2} \Gamma_0^{-2} \right] \quad \text{erg cm}^{-2} \text{ s}^{-1}, \quad (1)$$

where $F_{0.1}$ is the LAT flux from 100 MeV to 100 GeV in photons $\text{cm}^{-2} \text{ s}^{-1}$, $E_1 = 0.1$ GeV,

$E_2 = 100$ GeV, and $C_1 = 1.602 \times 10^{-3}$ erg GeV $^{-1}$, and Γ_0 is the γ -ray photon spectral index which is set to 2.1 for this calculation. Next, the luminosity was calculated using the equation

$$L_\gamma = \frac{4\pi D_L^2 S_{0.1}}{(1+z)^{2-\Gamma}} \text{ erg s}^{-1}, \quad (2)$$

where D_L is the luminosity distance¹ in cm and Γ is the γ -ray photon spectral index from 1LAC and 2LAC.

We calculated the radio luminosities using the equation

$$L_R = \frac{4\pi D_L^2 \nu S_\nu}{(1+z)} \text{ erg s}^{-1}, \quad (3)$$

where ν is 5 GHz, and S_ν is the total VLBA flux density we measured at 5 GHz. We assumed a flat radio spectrum index ($\alpha=0$) for the purposes of the k -correction and luminosity calculations.

The γ -ray loudness is then simply

$$G_{r,1FGL} = \frac{L_{\gamma,1FGL}}{L_R} \quad (4)$$

for 1FGL measurements and

$$G_{r,2FGL} = \frac{L_{\gamma,2FGL}}{L_R} \quad (5)$$

for 2FGL measurements.

All of our sources were significantly γ -ray loud. For the 1FGL data, the minimum $G_{r,1FGL}$ was 545 and the maximum was 187000, with an average value of 19500. For the 2FGL data, the minimum $G_{r,2FGL}$ was 404 and the maximum was 95100, with an average value of 13000. There are 2 possible explanations for this large change in maximum G_r and the significant change in average G_r : *i*) the 2FGL data were averaged over 2 years, so any sources in a high-activity/flaring state in the 11 months of 1FGL would naturally have lower γ -ray flux when averaged over a longer period of time, and *ii*) the 1 - 100 GeV flux was calculated slightly differently for 2FGL than in 1FGL (Nolan et al. 2011). We plot the 1FGL γ -ray versus radio luminosities in Figure 1. The 2FGL luminosities were very similar to the 1FGL luminosities.

Lister et al. (2011), reported a significant difference between the distributions of G_r for BL Lac objects and FSRQs. We did not find such a difference in our data. To examine the

¹We calculated our D_L values using a MATLAB® adaptation of Ned Wright's CosmoCalc program (Wright 2006).

likelihood that the BL Lac objects and FSRQs were unrelated, we used the Kolmogorov-Smirnov (K-S) test² (e.g., Press et al. 1986). The K-S test returned a 8% probability that the 1FGL BL Lac objects and FSRQs were drawn from the same parent population. For the 2FGL data, the K-S test result was 18%. See Figure 2 for a plot of the G_r distributions.

3.2. Peak Synchrotron Frequency

The frequency at which the synchrotron radiation is at a maximum (ν_{peak}^S) is typically found by making many measurements of the spectrum of a source and fitting a polynomial to these measurements (e.g., Nieppola et al. 2006). Ideally, one would like to have simultaneous multi-frequency measurements covering as much of the spectrum as possible. Unfortunately, such large simultaneous data are rarely available. When possible, we found estimates for ν_{peak}^S in the literature (see Table 1). It should also be noted that ν_{peak}^S is known to be variable (Rani et al. 2011). Therefore, we made an effort to use the most recent published data. We were able to find published ν_{peak}^S values for 102 of our sources, more than half of which came from Meyer et al. (2011).

If we could not find a published value of ν_{peak}^S , we employed the technique used in 2LAC. We used the average radio-optical (α_{RO}) and optical-x-ray (α_{OX}) spectral indices and the formula given in Abdo et al. (2010c).

$$\log(\nu_{peak}^S) = \begin{cases} 13.85 + 2.30X & \text{for } X < 0 \text{ and } Y < 0.3 \\ 13.15 + 6.58Y & \text{otherwise} \end{cases} \quad (6)$$

Here, $X = 0.565 - 1.433\alpha_{RO} + 0.155\alpha_{OX}$ and $Y = 1.0 - 0.661\alpha_{RO} - 0.339\alpha_{OX}$. As per Giommi et al. (2012a), the ν_{peak}^S for FSRQs was reduced by 0.5 in log space. Also, all ν_{peak}^S determined using the 2LAC method were expressed in the source rest frame. For those BL Lac objects without a measured redshift, the median BL Lac object redshift of 0.27 from the 2LAC was used, but only for the purposes of estimating ν_{peak}^S (i.e., we did not use this redshift to compute the luminosities). We used the 2LAC estimation method to find ν_{peak}^S values for 76 of our sources.

If we could not find a published value and the α_{RO} and/or α_{OX} numbers were not in 2LAC, we used flux measurements from the NASA/IPAC Extragalactic Database (NED)

²The K-S test is a useful statistic to determine the likelihood that two distributions are drawn from the same parent distribution. It is important to remember that K-S test results are only meaningful in determining if two distributions are different. That is, it should not be used to confirm that two distributions are similar, only that they are not drawn from the same parent population.

and fit a quadratic to the data in $\log(\nu F_\nu) - \log(\nu)$ space. Again, we used the most recent measurements available. The ν_{peak}^S 's found in this way are not as reliable as the 2LAC method, but they do tend to be reasonably close. To check the accuracy of the NED-fit method, we made fits for all of our sources. We threw out any fits that had less than 8 points for fitting and any that were obviously suspicious ($\nu_{peak,fit}^S < 12$ and $\nu_{peak,fit}^S > 19$), and then compared the remaining values to the published and 2LAC estimated values. We calculated how close the $\nu_{peak,fit}^S$ was by using

$$\Delta\% = \frac{|\nu_{peak}^S - \nu_{peak,fit}^S|}{\nu_{peak}^S} \times 100\% \quad (7)$$

The mean for $\Delta\%$ was 6.3%. The median was 3.7%. While this is not ideal, we feel it shows that the $\nu_{peak,fit}^S$'s are still acceptable estimates for those sources without a better alternative. We were able to obtain $\nu_{peak,fit}^S$ estimates for 28 of our sources: 18 FSRQs, 8 BL Lac objects, and 2 AGN/other objects. This brings our total number of sources with ν_{peak}^S values to 206.

As per the 1LAC convention, our sources were divided into 3 types based on their ν_{peak}^S : High-synchrotron peaked (HSP, $\nu_{peak}^S > 10^{15}$), Intermediate-synchrotron peaked (ISP, $10^{14} < \nu_{peak}^S < 10^{15}$), and low-synchrotron peaked (LSP, $\nu_{peak}^S < 10^{14}$). For brevity, we will refer to the HSP BL Lac objects as “HBLs”, ISP BL Lac objects as “IBLs”, and LSP BL Lac objects as “LBLs”. We had 42 LBLs, 24 IBLs, and 29 LBLs in our sample. We could not get good estimates of ν_{peak}^S for the remaining 11 BL Lac objects. For the FSRQs, 99 were LSP type, and 3 were ISP type. Notice that we do not have any HSP FSRQs in our sample. We could not get reliable ν_{peak}^S estimates for 12 of our FSRQs.

3.3. $G_r - \nu_{peak}^S$ Correlation

We applied the Spearman test³ (e.g., Press et al. 1986) to look for correlations between G_r and ν_{peak}^S in our data. We found mostly weak or tentative correlations for our sample. For the 1FGL data, the BL Lac objects had the only significant correlation with a ρ_s of 0.46 and a p of 4×10^{-4} . The FSRQs in the 1FGL data had a very tentative correlation with a ρ_s of 0.24 and a p of 0.02. We plot our 1FGL data in Figure 3. For the 2FGL data, both

³The nonparametric Spearman test returns a correlation coefficient (ρ_s), which has a range of $0 < |\rho_s| < 1$. A high value of $|\rho_s|$ indicates a significant correlation. The Spearman test also generates a significance (p). The smaller the value of p , the less likely the chances of obtaining the same ρ_s from random sampling. It is important to keep in mind that while the Spearman test is a powerful test for statistical correlation, it does not test an actual physical correlation.

the BL Lac objects and the FSRQs showed low-significance correlations. The 2FGL BL Lac objects had a ρ_S of 0.40 and a p of 0.003 while the FSRQs had a ρ_S of 0.28 and a p of 0.006.

The 1FGL result tentatively confirms the correlation by Lister et al. (2011) who found a good correlation for the BL Lac objects, and no correlation for the FSRQs. However, the low-significance results from the 2FGL data cast some doubt on the correlation for the BL Lac objects and also call into question whether or not there is a correlation for the FSRQs. Also, note that in Figure 3 we have a handful of sources with high ν_{peak}^S and relatively low G_r . With our large range in both, we do not suspect a selection effect here. However, Lister et al. (2011) had significantly fewer HBLs than we had in our sample (17 versus 30), so their result of a strong, positive correlation may have been caused by a selection effect. It does not seem to be caused by the fact that they were more biased towards high flux density objects. We limited our BL Lac object sample to those brighter than 200 mJy and again to those brighter than 100 mJy, and in both cases our correlations became weaker than when we used our full sample.

A strong correlation between G_r and ν_{peak}^S would indicate that the synchrotron self-Compton (SSC) model for γ -ray emission is more likely. That is, the seed photons for the inverse Compton scattering to γ -ray frequencies are internal to the source (i.e., provided by the synchrotron emission) and therefore both the synchrotron and inverse Compton emission have roughly the same Doppler factors. However, the fact that we see a lower significance correlation in the 2FGL data indicates that such a model may not be as accurate as previously thought. The tentative correlation between $G_{r,2FGL}$ and ν_{peak}^S for the FSRQs could indicate that at least some fraction of their inverse Compton emission is SSC, but their seed photon population may be enriched by photons external to the synchrotron emitting region (i.e., external inverse Compton scattering) such as the dusty torus or broad line region (BLR). Again, the low significance value for the correlation should make one cautious in drawing such a conclusion.

4. Results and Discussion

4.1. Total VLBA Flux Density

We found very strong correlations between the total VLBA flux density at 5 GHz and the synchrotron peak frequency for our BL Lac objects and FSRQs. The Spearman test result on the BL Lac objects was a ρ_S of -0.56 and a p of 5×10^{-9} . The results for the FSRQs were a ρ_S of -0.33 and a p of 7×10^{-4} . See Figure 4 for a plot of our flux density versus ν_{peak}^S . The $S_5 - \nu_{peak}^S$ correlation is expected for the BL Lac objects and was also seen

by Lister et al. (2011). The higher the ν_{peak}^S , the lower the radio flux density is going to be at 5 GHz which will contribute to a higher G_r . The FSRQs were not expected to show such a strong correlation. Lister et al. (2011) reported that their FSRQ sample showed no sign of correlation. It is possible that, because the MOJAVE program focuses on the brightest AGN, their sample did not contain enough low flux density objects to show a correlation. In fact, if we limit our FSRQ sample to those with $S_5 > 250$ mJy (excluding the 22 dimmest FSRQs with valid ν_{peak}^S 's), we no longer see a significant correlation ($\rho_S = -0.04$ and $p = 0.74$).

4.2. Gamma-ray Photon Spectral Index

Lister et al. (2011) reported a significant linear correlation between the γ -ray loudness and γ -ray photon spectral index for their BL Lac objects. We do not see a strong indication of this in our data. We used both 1FGL and 2FGL data, and only the 2FGL data showed any hint of this correlation. However, with a ρ_S of -0.25 and a p of 0.06, it is still too low a significance to claim a correlation in our sample. See Figure 5 for a plot of the 2FGL γ -ray loudness versus γ -ray photon spectral index. We should note that while our sample covers a very large range in G_r , we do not have the low G_r ($G_r < 100$) objects that Lister et al. (2011) had in their sample. It is possible that adding these low G_r sources would lead to a strong correlation.

However, we do confirm the correlation between γ -ray luminosity and γ -ray photon spectral index reported by Ghisellini et al. (2009) and Chen & Bai (2011). For the 1FGL data, the Spearman test gives a ρ_S of 0.43 and a p of 2×10^{-9} for the full sample. The 2FGL data also showed a correlation with a ρ_S of 0.35 and a p of 4×10^{-6} . Breaking the sources up by type, only the BL Lac objects show a correlation in either 1FGL ($\rho_S = 0.54$, $p = 8 \times 10^{-6}$) or 2FGL ($\rho_S = 0.50$, $p = 10^{-4}$). See Figure 6 for a plot of the 1FGL γ -ray photon spectral index versus γ -ray luminosity (the 2FGL plot looks similar and is not shown). Ghisellini et al. (2009) and Chen & Bai (2011) argue that this correlation indicates that the low-luminosity-low- ν_{peak}^S sources have lower black hole masses than the high-luminosity-high- ν_{peak}^S sources. That is, the black hole mass, not beaming, may be responsible for the observed properties of low-luminosity LBLs. However, our results from investigating the core brightness temperature and variability (below) do not support this.

4.3. Core Brightness Temperature

We found a correlation between the core brightness temperature and the peak synchrotron frequency for our sources. When we applied the Spearman test to the entire sample, we found a ρ_S value of -0.40 and a p of 4×10^{-9} . However, when we broke the sample up by optical type, only the BL Lac objects showed a significant correlation ($\rho_S = -0.55$, $p = 10^{-8}$). See Figure 7 for a plot of the core brightness temperature versus ν_{peak}^S . High core brightness temperatures are generally associated with large Doppler factors (e.g., Tingay et al. 2001). Therefore, it would seem that the LBLs are more strongly beamed than the HBLs. Recall from Section 5.3 that the HBLs also tend to have larger G_r . Combining their high G_r and low core brightness temperatures indicates that the HBLs are probably more efficient at producing γ -rays. The LBLs, on the other hand, may be seen as γ -ray loud thanks to higher Doppler factors. Lister et al. (2011) did not report finding a correlation between core brightness temperature and ν_{peak}^S , but they did note that their HBLs tended to have lower core brightness temperatures than the IBLs and LBLs.

4.4. Apparent Jet Opening Angle

We measured the mean apparent opening half angle for each source with core-jet morphology following the procedure described in Taylor et al. (2007). This method relies on averaging the apparent opening angles found for each jet component in a source. That is, the apparent opening angle is measured for several (more than 2) jet components. The half-opening angle is calculated for each component to be

$$\psi = \arctan[(|y'| + dr)/|x'|] \quad (8)$$

where x' and y' are the positions of the component in a rotated coordinate system with the x' -axis aligned with the jet axis, and dr is the deconvolved Gaussian size perpendicular to the jet axis. The final mean opening angle for the source is the average of all of the opening angles for the individual jet components.

Lister et al. (2011) reported a non-linear correlation between the opening angle and the γ -ray loudness. We found a tentative correlation, however only when we used the 2FGL data. When we performed the Spearman test on all 33 sources with both a measured opening angle and a 2FGL γ -ray flux (including the radio galaxy NGC 6251), we found a ρ_S of 0.57 and a p of 5×10^{-4} . When we break the sources up by type, we only see a tentative correlation for the FSRQs ($\rho_S=0.62$, $p=0.004$), however the sample sizes are very small. We only had 36 objects with opening angle and G_r measurements in 1FGL, and 33 in 2FGL. The sample in Lister et al. (2011), on the other hand, contained well over 100 sources. See Figure 8 for

a plot of the 2FGL γ -ray loudness versus opening angle. We should also note that Lister et al. (2011) made their measurements of the apparent opening angle using mean sizes of jet components over several epochs, not the mean of multiple apparent opening angles from several components in a single observation as we did. The fact that MOJAVE is a monitoring program makes it much better suited to investigating the apparent (and intrinsic) opening angles than our sample.

4.5. Polarization

To measure the polarization properties of our sources, we used the Gaussian mask method described by Helmboldt et al. (2007). With this method, mask images were created using the Gaussian fit components in the Stokes I image to define the core and jet components. We then created mask images using the polarized intensity maps and mask out any pixels that do not have a signal-to-noise of at least 5 (compared to the noise image generated by the AIPS task COMB). The two mask types were then combined (multiplied) and applied to both the Stokes I and polarized intensity maps. Additionally, in order to be considered “polarized”, a source had to have a polarized flux of at least 0.3% of the Stokes I peak value (to avoid leakage contamination). See Linford et al. (2012) for more discussion on the polarization properties of our sources.

Lister et al. (2011) reported that the HBLs in their sample tended to have lower core fractional polarization levels. We also see an indication of this in our sample. Our Spearman test returned only a very marginal correlation between core fractional polarization and ν_{peak}^S for the BL Lac objects, with a ρ_S value of -0.25 and a p of 0.04. However, we do note that the maximum HBL core fractional polarization is definitely less than the maximum for the IBLs or LBLs. We did not find any correlation between core fractional polarization and ν_{peak}^S for the FSRQs (see Figure 9 for a plot).

4.6. Radio Variability

It is well known that blazars tend to be highly variable sources. It is believed that this variability is related to Doppler beaming (e.g., Hovatta et al. 2009) because small changes in bulk material velocity and/or orientation angle can lead to large changes in the observed flux. It has also been shown that Doppler beaming can shorten the apparent timescales of flaring events (e.g., Lister 2001). We used the modulation index from the Owens Valley Radio Observatory (OVRO) blazar monitoring program (Richards et al. 2011) as a measure

of our sources variability. The modulation index is the standard deviation of the distribution of source flux densities in time divided by the mean flux density. Our sample and the OVRO sample had 120 sources in common. Richards et al. (2011) reported that the FSRQs in their sample tended to have larger variability than the BL Lac objects. We did not see strong evidence for this in our sample, but we should note that our sample is considerably smaller than Richards et al. (2011). However, we did find that the HBLs tend to have relatively low variability (see Figure 10). We also found a tentative correlation between the modulation index and ν_{peak}^S for the both the BL Lac objects and the FSRQs. The Spearman test results for the BL Lac objects were a ρ_S of -0.33 and a p of 0.02. This is another indication that the HBLs may not be as strongly beamed as the LBLs. Interestingly, the FSRQs showed tentative positive correlation with a ρ_S of 0.34 and a p of 0.007. However, it is hard to convince oneself that such a correlation exists for the FSRQs by examining Figure 10.

4.7. Favoring 2LAC Estimates of Peak Synchrotron Frequency

As we mentioned in Section 3.2, we opted to use the most recent published values of ν_{peak}^S when available. However, it is likely that there were variations in how those values were determined in different studies. An alternative to using recent published values is to use the 2LAC estimation method for as many sources as possible, and fill in the blanks with published and NED-fit values. While the 2LAC method has been shown to be a reasonable estimate of ν_{peak}^S , it is still an empirical estimate and does not always agree well with values calculated from fitting the SEDs.

We created a second data set favoring the 2LAC estimates of ν_{peak}^S and applied the Spearman test again to look for correlation. For this secondary data set, we used the 2LAC estimated ν_{peak}^S values for 165 of our sources. We also used 13 published values and 28 NED-fit values when the 2LAC estimation could not be calculated. In general, the correlations reported above were still present, but with slightly reduced ρ_S values (indicating weaker correlation) and increased p values (indicating less significant correlation). We did find a handful of significant differences when relying on the 2LAC values. First, the FSRQs do not show any significant correlation for G_R and ν_{peak}^S in either 1FGL or 2FGL. Second, we no longer see any significant correlation between ν_{peak}^S and core fractional polarization for the BL Lac objects. Finally, we no longer see any correlation between ν_{peak}^S and the modulation index (variability) for either BL Lac objects or FSRQs. It should be noted that all the correlations that disappeared when relying on the 2LAC ν_{peak}^S estimates were marginal or tentative correlations using the published ν_{peak}^S values.

5. Misidentified BL Lac Objects?

It has recently been argued that some of the low-synchrotron BL Lac objects may not actually be BL Lac objects (e.g., Ghisellini et al. 2009, Giommi et al. 2012a). In fact, it is possible that BL Lacertae itself is not actually a BL Lac object (Vermeulen et al. 1995). The argument made is that some objects classified as LBLs are actually FSRQs with exceptionally strong jets and the broad line region (BLR) is simply not visible due to the jet emission overpowering the emission from the BLR (or, more familiarly, the jet is “swamping” the BLR). The lack of obvious broad lines leads the astronomical community to mis-classify some sources as BL Lac objects.

To investigate this possibility, we compared the LBLs to the combined HBL+IBL population and to the FSRQs. We looked at every parameter we had measured, and found that there are indeed several instances where the LBLs appear to be very different from the rest of the BL Lacs and are more like the FSRQs. In particular, the distributions of the total VLBA radio flux density (see Figure 11) showed significant difference between the LBLs and the rest of the BL Lac objects. We applied the K-S test to the distributions of total radio flux density and found that the probability of the LBLs and HBL+IBLs being drawn from the same parent sample was 6×10^{-8} . The core brightness temperatures for LBLs are also very unlike the core brightness temperatures of the rest of the BL Lac objects (see Figure 12). The K-S test result for the core brightness temperatures was a probability of 6×10^{-5} that the LBLs and HBL+IBLs were drawn from the same parent sample.

Interestingly, the K-S tests on the 1FGL and 2FGL γ -ray loudness distributions seem to indicate that the LBLs are not related to either the IBL+HBL or the FSRQ populations. The apparent opening angle distributions were the only example where the LBLs showed strong likelihood of being unlike the FSRQs while not being very different from the IBL+HBL population. However, this may simply be the result of low-number statistics.

Lister et al. (2011) found a difference between the core fractional polarization between the LBLs and HBLs. We do not see any strong evidence for this in our sample. However, we should note that we do not use lower limits on our “unpolarized” sources, whereas the MOJAVE group did (Talvikki Hovatta, private communication). Recall that we set “unpolarized” sources to have a core fractional polarization of 0% and we only included sources with non-zero core fractional polarization in our “polarized” sample. Therefore, we will naturally have different results than if we had included lower limits on those sources.

Lister et al. (2011) argued that their $G_r - \nu_{peak}^S$ correlation for BL Lac objects indicates that the LBLs and HBLs should belong to the same parent population. However, we would argue that having some contamination of FSRQs masquerading as LBLs would not

necessarily destroy any statistical correlation. Furthermore, we did not find as strong of a $G_r - \nu_{peak}^S$ correlation for the BL Lac objects in our data. To test our hypothesis that adding FSRQs to the LBL population would not destroy a statistical $G_r - \nu_{peak}^S$ correlation, we created contaminated samples by deliberately including known LSP FSRQs in our BL Lac object sample. We then used the Spearman test to look for correlation in the contaminated samples. Using 1FGL data, we found that after increasing the LBL sample size by 25% with contaminating LSP FSRQs, the correlation results did not change significantly, and the correlation is still tentative after increasing the LBL sample size by 50% and 100%. Using 2FGL data, the correlation becomes tentative after increasing the LBL sample size by 25%, but it remains a tentative correlation even after increasing the LBL sample size by 50% and 100%. See Table 2 for our full results.

While we cannot say for certain that we have some FSRQs masquerading as LBLs, it does seem likely. Unfortunately, we cannot separate the misidentified BL Lac objects from the real ones just yet. This will require monitoring these LBLs and watching for ones that have a drop in jet power leading to detection of a BLR (Vermeulen et al. 1995).

6. Summary and Conclusions

We have analyzed a sample of 232 LAT-detected AGN using both 1FGL and 2FGL data to compare our results with those of Lister et al. (2011). All of the sources in our sample are significantly γ -ray loud. We did not find a significant difference between the distributions of G_r for BL Lac objects and FSRQs. Using 1FGL data, we find a weak correlation between G_r and ν_{peak}^S for the BL Lac objects and a tentative correlation for the FSRQs. Using 2FGL, we found a very tentative $G_r - \nu_{peak}^S$ correlation for both FSRQs and BL Lac objects.

Looking at the parsec-scale radio properties of our sources, we find a very strong correlation between total VLBA flux density and ν_{peak}^S for both BL Lac objects and FSRQs. We could not confirm the correlation between G_r and the γ -ray photon index reported by Lister et al. (2011), but we did confirm the correlation between γ -ray luminosity and γ -ray photon index reported by other groups. We also found a very strong correlation between the core brightness temperatures and ν_{peak}^S for BL Lac objects. Although we had a limited sample of apparent jet opening angle measurements, we were still able to tentatively confirm the correlation with G_r reported by Lister et al. (2011). We did not find any evidence of a correlation between core fractional polarization and ν_{peak}^S . We found a tentative negative correlation between radio variability (modulation index) and ν_{peak}^S for the BL Lac objects and a tentative positive correlation for the FSRQs. The fact that the core brightness temperature shows a positive correlation with ν_{peak}^S and modulation index shows a negative correlation

with ν_{peak}^S indicates that the LBLs are more strongly beamed than the IBLs and HBLs.

The LBLs in our sample often appear to be different for the rest of the BL Lac objects. In particular, we found significant differences in the distributions of core brightness temperatures and total VLBA flux density. It seems likely, therefore, that our LBL population contains some misidentified FSRQs which may have their BLR swamped by their jet emission. While Lister et al. (2011) argued that a G_r - ν_{peak}^S correlation for the BL Lac objects indicated that the LBLs were related to the IBLs and HBLs, we found that deliberately contaminating our LBL sample with known FSRQs did not change our (albeit weak) correlation significantly.

Future studies of large samples of blazars, which should include both very high and low flux density objects, should be conducted to further investigate the relationships between G_r , ν_{peak}^S , and the parsec-scale radio properties. Long-term monitoring of LBLs may also present clear evidence that some of these objects are actually FSRQs.

We thank the anonymous referee for their constructive criticism and helpful comments on this manuscript. We thank Talvikki Hovatta for useful discussions regarding MOJAVE core fractional polarization measurements and Roger Romani for useful discussions about the 2LAC synchrotron peak frequency estimation method. The National Radio Astronomy Observatory is a facility of the National Science Foundation operated under cooperative agreement by Associated Universities, Inc. The VLBA is a facility of the National Science Foundation operated by the National Radio Astronomy Observatory under cooperative agreement by Associated Universities, Inc. MATLAB is a registered trademark of The MathWorks, Inc. (Natick, Massachusetts, USA). The NASA/IPAC Extragalactic Database (NED) is operated by the Jet Propulsion Laboratory, California Institute of Technology, under contract with the National Aeronautics and Space Administration. We thank NASA for support under FERMI grant GSFC #21078/FERMI08-0051, and the NRAO for support under Student Observing Support Award GSSP10-011. Additional support provided by the Naval Research Laboratory.

REFERENCES

- Aatrokoski, J., Ade, P. A. R., Aghanim, N., et al. 2011, *A&A*, 536, 15
 Abdo, A. A., Ackermann, M., Ajello, M., et al. 2010a, *ApJS*, 188, 405
 Abdo, A. A., Ackermann, M., Ajello, M., et al. 2010b, *ApJ*, 715, 429
 Abdo, A. A., Ackermann, M., Agudo, I., et al., 2010c, *ApJ*, 716, 30
 Ackermann, M., Ajello, M., Allafort, A., et al. 2011, *ApJ*, 743, 171

- Atwood, B. W., Abdo, A. A., Ackermann, M., et al. 2009, *ApJ*, 697, 1071
- Chen, L., & Bai, J. M. 2011, *ApJ*, 735, 108
- Fossati, G., Maraschi, L., Celotti, A., et al. 1998, *MNRAS*, 299, 433
- Ghisellini, G., Celotti, A., Fossati, G., et al. 1998, *MNRAS*, 301, 451
- Ghisellini, G., & Tavecchio, F. 2008, *MNRAS*, 387, 1669
- Ghisellini, G., Maraschi, L., & Tavecchio, F. 2009, *MNRAS*, 396, L105
- Giommi, P., Padovani, P., Polenta, G., Turriziani, S., D’Elia, V., & Piranomonte, S. 2012a, *MNRAS*, 420, 2899
- Giommi, P., Polenta, G., Lähteenmäki, A., et al. 2012b, *A&A*, 541, 160
- Helmboldt, J. F., Taylor, G. B., Tremblay, S., et al. 2007, *ApJ*, 658, 203
- Hinshaw, G., Weiland, J. L., Hill, R. S., et al. 2009, *ApJS*, 180, 225
- Homan, D. C., Kadler, M., Kellermann, K. I., et al. 2009, *ApJ*, 706, 1253
- Hovatta, T., Valtaoja, E., Tornikoski, M., & Lähteenmäki, A. 2009, *A&A*, 498, 723
- Linford, J. D., Taylor, G. B., Romani, R. W., et al. 2011, *ApJ*, 726, 16
- Linford, J. D., Taylor, G. B., Romani, R. W., Helmboldt, J. F., Readhead, A. C. S., Reeves, R., & Richards, J. L. 2012, *ApJ*, 744, 177
- Lister, M. L. 2001, *ApJ*, 561, 676
- Lister, M. L., Cohen, M. H., Homan, D. C., et al. 2009a, *AJ*, 138, 1874
- Lister, M. L., Aller, H. D., Aller, M. F., et al. 2009b, *AJ*, 137, 3718
- Lister, M. L., Aller, M., Aller, H., et al. 2011, *ApJ*, 742, 27
- Marscher, A. P. 2006, *AIP Conf. Proc.* 856: Relativistic Jets: The Common Physics of AGN, Microquasars, and Gamma-Ray Bursts, 856, 1
- Meyer, E. T., Fossati, G., Georganopoulos, M., & Lister, M. L. 2011, *ApJ*, 740, 98
- Nieppola, E., Tornikoski, M., & Valtaoja, E. 2006, *A&A*, 445, 441
- Nieppola, E., Valtaoja, E., Tornikoski, M., Hovatta, T., & Kotiranta, M. 2008, *A&A*, 488, 867
- Nolan, P. L., Abdo, A. A., Ackermann, M., et al. 2012, *ApJS*, 199, 31
- Press, W. H., Flannery, B. P., Teukolsky, S. A., & Vetterlin, W. T. 1986, *Numerical Recipes: The Art of Scientific Computing* (Cambridge University Press)
- Rani, B., Gupta, A. C., Bachev, R., et al. 2011, *MNRAS*, 417, 1881

- Richards, J. L., Max-Moerbeck, W., Pavlidou, V., et al. 2011, ApJS, 194, 29
- Taylor, G. B., Healey, S. E., Helmboldt, J. F., et al. 2007, ApJ, 671, 1355
- Tingay, S. J., Preston, R. A., Lister, M. L., et al. 2001, ApJ, 549, L55
- Urry, C. M. & Padovani, P. 1995, PASP, 107, 803
- Vermeulen, R. C., Ogle, P. M., Tran, H. D., et al. 1995, ApJ, 452, L5
- Wright, E. L. 2006, PASP, 118, 1711

Table 1. Source Data

Source Name	1FGL Name	2FGL Name	Alternate AGN Name	Opt. Type	SED Type	SED Ref	$G_{r,1FGL}$	$G_{r,2FGL}$
F00057+3815	1FGL J0005.7+3815	2FGL J0006.1+3821	B2 0003+38A	bzq	LSP	2LAC	4675	3412
F00193+2017	1FGL J0019.3+2017	...	PKS 0017+200	bzb	LSP	N-06
F00230+4453	1FGL J0023.0+4453	2FGL J0023.2+4454	B3 0020+446	bzq	41162	15615
F00419+2318	1FGL J0041.9+2318	...	PKS 0039+230	bzq	LSP	fit	6226	...
F00580+3314	1FGL J0058.0+3314	2FGL J0057.9+3311	CRATES J0058+3311	bzb	33541	13762
F01022+4223	1FGL J0102.2+4223	2FGL J0102.3+4216	CRATES J0102+4214	bzq	29901	18855
F01090+1816	1FGL J0109.0+1816	2FGL J0109.0+1817	CRATES J0109+1816	bzb	HSP	2LAC	13338	9149
F01120+2247 ^M	1FGL J0112.0+2247	2FGL J0112.1+2245	CGRaBS J0112+2244	bzb	LSP	M-11	11084	11018
F01129+3207 ^M	1FGL J0112.9+3207	2FGL J0112.8+3208	4C +31.03	bzq	LSP	2LAC	26411	14138
F01138+4945	1FGL J0113.8+4945	2FGL J0113.7+4948	CGRaBS J0113+4948	bzq	LSP	2LAC	4411	2373
F01144+1327	1FGL J0114.4+1327*	2FGL J0114.7+1326**	CRATES J0113+1324	bzb	34296	16980
F01370+4751 ^M	1FGL J0137.0+4751	2FGL J0136.9+4751	OC 457	bzq	LSP	M-11	5722	2894
F01446+2703	1FGL J0144.6+2703	2FGL J0144.6+2704	CRATES J0144+2705	bzb	LSP	2LAC
F02035+7234	1FGL J0203.5+7234	2FGL J0203.6+7235	CGRaBS J0203+7232	bzb	LSP	N-06
F02045+1516	1FGL J0204.5+1516	2FGL J0205.0+1514	4C +15.05	agn	LSP	M-11	1324	866
F02053+3217 ^M	1FGL J0205.3+3217	2FGL J0205.4+3211	B2 0202+31	bzq	LSP	2LAC	4006	1803
F02112+1049	1FGL J0211.2+1049	2FGL J0211.2+1050	CGRaBS J0211+1051	bzb	ISP	2LAC
F02178+7353 ^M	1FGL J0217.8+7353	2FGL J0217.7+7353	1ES 0212+735	bzq	LSP	M-11	7096	3217
F02210+3555	1FGL J0221.0+3555	2FGL J0221.0+3555	B2 0218+35	bzq	LSP	N-08	14719	11023
F02308+4031	1FGL J0230.8+4031	2FGL J0230.8+4031	B3 0227+403	bzq	LSP	fit	11845	13164
F02379+2848	1FGL J0237.9+2848	2FGL J0237.8+2846	4C +28.07	bzq	LSP	M-11	7632	3598
F02386+1637	1FGL J0238.6+1637	2FGL J0238.7+1637	PKS 0235+164	bzb	LSP	M-11	39868	17005
F02435+7116	1FGL J0243.5+7116	2FGL J0242.9+7118	CRATES J0243+7120	bzb	HSP	N-06
F02454+2413	1FGL J0245.4+2413	2FGL J0245.1+2406	B2 0242+23	bzq	LSP	2LAC	38503	35651
F02580+2033	1FGL J0258.0+2033	2FGL J0257.9+2025 ^c	CRATES J0258+2030	bzb	HSP	2LAC
F03106+3812	1FGL J0310.6+3812	2FGL J0310.7+3813	B3 0307+380	bzq	LSP	2LAC	10251	5742
F03197+4130 ^M	1FGL J0319.7+4130	2FGL J0319.8+4130	NGC 1275	agn	LSP	M-11	545	404
F03250+3403	1FGL J0325.0+3403	2FGL J0324.8+3408	B2 0321+33B	...	HSP	2LAC	6861	3899
F03259+2219	1FGL J0325.9+2219	2FGL J0326.1+2226	CGRaBS J0325+2224	bzq	LSP	2LAC	18438	10045
F03546+8009	1FGL J0354.6+8009	2FGL J0354.1+8010	CRATES J0354+8009	agu	LSP	2LAC
F04335+2905 ^M	1FGL J0433.5+2905	2FGL J0433.5+2905	CGRaBS J0433+2905	bzb	LSP	2LAC
F04335+3230	1FGL J0433.5+3230	2FGL J0433.7+3233	CRATES J0433+3237	bzq	26569	35011
F04406+2748	1FGL J0440.6+2748	2FGL J0440.9+2749	B2 0437+27B	bzb
F04486+112A	1FGL J0448.6+1118*	2FGL J0448.9+1121**	CRATES J0448+1127	bzq	LSP	M-11	23877	20659
F04486+112B	1FGL J0448.6+1118*	2FGL J0448.9+1121**	PKS 0446+11	bzb	LSP	N-08	6522	5801
F05092+1015	1FGL J0509.2+1015	2FGL J0509.2+1013	PKS 0506+101	bzq	13083	6456
F05100+180A	1FGL J0510.0+1800*	2FGL J0509.9+1802	CRATES J0509+1806	agu

Table 1—Continued

Source Name	1FGL Name	2FGL Name	Alternate AGN Name	Opt. Type	SED Type	SED Ref	$G_{r,1FGL}$	$G_{r,2FGL}$
F05100+180B	1FGL J0510.0+1800*	2FGL J0509.9+1802	PKS 0507+17	bzq	LSP	N-08	4989	5028
F05310+1331 ^M	1FGL J0531.0+1331	2FGL J0530.8+1333	PKS 0528+134	bzq	LSP	M-11	16680	5733
F06072+4739	1FGL J0607.2+4739	2FGL J0607.4+4739	CGRaBS J0607+4739	bzb	ISP	2LAC
F06127+4120 ^M	1FGL J0612.7+4120	2FGL J0612.8+4122	B3 0609+413	bzb
F06169+5701	1FGL J0616.9+5701	2FGL J0616.9+5701	CRATES J0617+5701	bzb	ISP	2LAC
F06254+4440	1FGL J0625.4+4440	2FGL J0625.2+4441	CGRaBS J0625+4440	bzb	LSP	N-06
F06399+7325	1FGL J0639.9+7325	...	CGRaBS J0639+7324	bzq	LSP	M-11	15294	6293
F06507+2503	1FGL J0650.7+2503	2FGL J0650.7+2505	1ES 0647+250	bzb	HSP	N-06	37931	33759
F06544+5042 ^M	1FGL J0654.4+5042	2FGL J0654.5+5043	CGRaBS J0654+5042	agu	LSP	2LAC
F06543+4514	1FGL J0654.3+4514	2FGL J0654.2+4514	B3 0650+453	bzq	LSP	2LAC	51289	21437
F07114+4731	1FGL J0711.4+4731	2FGL J0710.8+4733	B3 0707+476	bzb	ISP	M-11	8555	5361
F07127+5033	1FGL J0712.7+5033	2FGL J0712.9+5032	CGRaBS J0712+5033	bzb	LSP	2LAC
F07193+3306 ^M	1FGL J0719.3+3306	2FGL J0719.3+3306	B2 0716+33	bzq	LSP	M-11	14239	11954
F07219+7120 ^M	1FGL J0721.9+7120	2FGL J0721.9+7120	CGRaBS J0721+7120	bzb	ISP	M-11	6111	6947
F07253+1431	1FGL J0725.3+1431	2FGL J0725.3+1426	4C +14.23	bzq	LSP	2LAC	6305	14005
F07382+1741 ^M	1FGL J0738.2+1741	2FGL J0738.0+1742	PKS 0735+178	bzb	LSP	M-11	3995	4161
J07426+5444	1FGL J0742.2+5443	2FGL J0742.6+5442	CRATES J0742+5444	bzq	LSP	2LAC	22776	16690
J07464+2549	1FGL J0746.6+2548	2FGL J0746.6+2549	B2 0743+25	bzq	LSP	2LAC	32807	29470
F07506+1235 ^M	1FGL J0750.6+1235	2FGL J0750.6+1230	PKS 0748+126	bzq	LSP	M-11	1087	1058
J07530+5352	1FGL J0752.8+5353	2FGL J0753.0+5352	4C +54.15	bzb	LSP	2LAC	2524	1522
J08053+6144	1FGL J0806.2+6148	2FGL J0805.5+6145	CGRaBS J0805+6144	bzq	LSP	2LAC	23584	22464
J08096+3455	1FGL J0809.4+3455	...	B2 0806+35	bzb	6568	...
J08098+5218	1FGL J0809.5+5219	2FGL J0809.8+5218	CRATES J0809+5218	bzb	HSP	M-11	16425	8916
J08146+6431	1FGL J0815.0+6434	2FGL J0814.7+6429	CGRaBS J0814+6431	bzb	ISP	2LAC
J08163+5739	1FGL J0816.7+5739	2FGL J0816.5+5739	BZB J0816+5739	bzb	HSP	M-11
J08182+4222 ^M	1FGL J0818.2+4222	2FGL J0818.2+4223	B3 0814+425	bzb	LSP	M-11	4287	3029
J08247+5552	1FGL J0825.0+5555	2FGL J0824.9+5552	OJ 535	bzq	LSP	2LAC	13192	6045
J08308+2410 ^M	1FGL J0830.5+2407	2FGL J0830.5+2407	OJ 248	bzq	LSP	M-11	7625	4792
J08338+4224	1FGL J0834.4+4221	2FGL J0834.3+4221	B3 0830+425	bzq	6741	3237
F08422+7054 ^M	1FGL J0842.2+7054	2FGL J0841.6+7052	4C +71.07	bzq	LSP	M-11	14357	12236
F08499+4852	1FGL J0849.9+4852	2FGL J0849.8+4852	CRATES J0850+4854	agu	ISP	2LAC
J08548+2006 ^M	1FGL J0854.8+2006	2FGL J0854.8+2005	OJ 287	bzb	LSP	M-11	1574	1041
J08566+2057	1FGL J0856.6+2103*	...	CRATES J0850+2057	bzq	56614	...
J08569+2111	1FGL J0856.6+2103*	...	OJ 290	bzq	LSP	fit	16425	...
F09055+1356	1FGL J0905.5+1356	2FGL J0905.6+1357	CRATES J0905+1358	agu
J09106+3329	1FGL J0910.7+3332	2FGL J0910.6+3329	Ton 1015	bzb	HSP	N-06	10457	5898
J09121+4126	1FGL J0912.3+4127	2FGL J0912.1+4126	B3 0908+416B	bzq	LSP	2LAC	25612	20286

Table 1—Continued

Source Name	1FGL Name	2FGL Name	Alternate AGN Name	Opt. Type	SED Type	SED Ref	$G_{r,1FGL}$	$G_{r,2FGL}$
J09158+2933	1FGL J0915.7+2931	2FGL J0915.8+2932	B2 0912+29	bzb	HSP	M-11
J09209+4441 ^M	1FGL J0920.9+4441	2FGL J0920.9+4441	B3 0917+449	bzq	LSP	A-11	42956	19211
J09216+6215	1FGL J0919.6+6216	2FGL J0921.9+6216	OK 630	bzq	LSP	M-11	4340	2528
J09235+4125	1FGL J0923.2+4121	2FGL J0923.2+4125	B3 0920+416	agn	LSP	fit	7086	3410
J09238+2815	1FGL J0924.2+2812	2FGL J0924.0+2819	B2 0920+28	bzq	LSP	fit	4228	3076
J09292+5013	1FGL J0929.4+5000	2FGL J0929.5+5009	CRATES J0929+5013	bzb	LSP	M-11	2503	1761
J09341+3926	1FGL J0934.5+3929	2FGL J0934.7+3932	CGRaBS J0934+3926	bzb	LSP	fit	8100	5579
J09372+5008	1FGL J0937.7+5005	2FGL J0937.6+5009	CGRaBS J0937+5008	bzq	LSP	2LAC	9429	3135
J09418+2728	1FGL J0941.2+2722	2FGL J0941.4+2724 [*]	CGRaBS J0941+2728	bzq	LSP	fit	10411	6734
F09456+5754	1FGL J0945.6+5754	2FGL J0945.9+5751	CRATES J0945+5757	bzb	LSP	fit	20374	13578
F09466+1012	1FGL J0946.6+1012	2FGL J0946.5+1015	CRATES J0946+1017	bzq	ISP	fit	12803	11436
J09496+1752	1FGL J0949.8+1757 [*]	...	CRATES J0949+1752	bzq	8191	...
F09498+1757	1FGL J0949.8+1757 [*]	...	CRATES J0950+1804	agu	LSP	fit	45589	...
F09565+6938	1FGL J0956.5+6938	2FGL J0955.9+6936	M 82	sbq	ISP	2LAC	104237	54147
J09568+2515	1FGL J0956.9+2513	2FGL J0956.9+2516	B2 0954+25A	bzq	LSP	M-11	3690	2897
J09576+5522 ^M	1FGL J0957.7+5523	2FGL J0957.7+5522	4C +55.17	bzq	LSP	M-11	14326	8662
F10001+6539 ^M	1FGL J1000.1+6539	...	CGRaBS J0958+6533	bzb	LSP	A-11	1247	...
F10127+2440 ^M	1FGL J1012.7+2440	2FGL J1012.6+2440	CRATES J1012+2439	bzq	ISP	0FGL	118387	94741
J10150+4926 ^M	1FGL J1015.1+4927	2FGL J1015.1+4925	1ES 1011+496	bzb	ISP	M-11	14129	8908
J10330+4116	1FGL J1033.2+4116	2FGL J1033.2+4117	B3 1030+415	bzq	LSP	M-11	2693	2370
J10338+6051	1FGL J1033.8+6048	2FGL J1033.9+6050	CGRaBS J1033+6051	bzq	LSP	2LAC	38586	37310
F10377+5711 ^M	1FGL J1037.7+5711	2FGL J1037.6+5712	CRATES J1037+5711	bzb	LSP	M-11
J10431+2408	1FGL J1043.1+2404	2FGL J1043.1+2404	B2 1040+24A	bzb	LSP	N-08	1455	1435
F10487+8054	1FGL J1048.7+8054	...	CGRaBS J1044+8054	bzq	LSP	N-08	14738	...
F10485+7239	1FGL J1048.5+7239	2FGL J1049.7+7240	CRATES J1047+7238	agu
F10488+7145	1FGL J1048.8+7145	2FGL J1048.3+7144	CGRaBS J1048+7143	bzq	LSP	2LAC	5867	4236
J10586+5628 ^M	1FGL J1058.6+5628	2FGL J1058.6+5628	CGRaBS J1058+5628	bzb	HSP	N-06	15262	10747
J11044+3812 ^M	1FGL J1104.4+3812	2FGL J1104.4+3812	Mkn 421	bzb	HSP	M-11	25649	24131
J11061+2812	1FGL J1106.5+2809	2FGL J1106.1+2814	CRATES J1106+2812	agu	LSP	2LAC	13858	5629
J11126+3446	1FGL J1112.8+3444	2FGL J1112.4+3450	CRATES J1112+3446	bzq	ISP	fit	31922	25768
F11171+2013	1FGL J1117.1+2013	2FGL J1117.2+2013	CRATES J1117+2014	bzb	HSP	2LAC	12285	15630
J11240+2336	1FGL J1123.9+2339	2FGL J1124.2+2338	OM 235	bzb	LSP	fit
F11366+7009	1FGL J1136.6+7009	2FGL J1136.7+7009	Mkn 180	bzb	HSP	M-11	3793	2143
J11421+1547	1FGL J1141.8+1549	2FGL J1141.9+1550	CRATES J1142+1547	agu	LSP	fit
J11469+3958	1FGL J1146.8+4004	2FGL J1146.9+4000	B2 1144+40	bzq	LSP	fit	8904	6644
J11503+2417	1FGL J1150.2+2419	2FGL J1150.1+2419	B2 1147+24	bzb	LSP	M-11	2323	1345
J11514+5859	1FGL J1151.6+5857	2FGL J1151.5+5857	CRATES J1151+5859	bzb	HSP	M-11

Table 1—Continued

Source Name	1FGL Name	2FGL Name	Alternate AGN Name	Opt. Type	SED Type	SED Ref	$G_{r,1FGL}$	$G_{r,2FGL}$
J11540+6022	1FGL J1152.1+6027	2FGL J1154.4+6019	CRATES J1154+6022	...	LSP	M-11
J11595+2914 ^M	1FGL J1159.4+2914	2FGL J1159.5+2914	4C +29.45	bzq	LSP	M-11	7871	6459
J12030+6031	1FGL J1202.9+6032	2FGL J1203.2+6030	CRATES J1203+6031	agn	ISP	2LAC	12362	6094
J12089+5441	1FGL J1209.3+5444	2FGL J1208.8+5441	CRATES J1208+5441	bzq	LSP	fit	28188	23684
J12093+4119	1FGL J1209.4+4119	2FGL J1209.6+4121	B3 1206+416	bzb	ISP	N-06	8644	2661
J12098+1810	1FGL J1209.7+1806	2FGL J1209.7+1807	CRATES J1209+1810	bzq	LSP	fit	12218	13096
J12178+3007 ^M	1FGL J1217.7+3007	...	B2 1215+30	bzb	HSP	M-11	13652	...
F12215+7106	1FGL J1221.5+7106	2FGL J1219.2+7107	CRATES J1220+7105	bzq	3189	2413
J12201+3431	1FGL J1220.2+3432	...	CGRaBS J1220+3431	bzb	ISP	N-06	5198	...
J12215+2813 ^M	1FGL J1221.5+2814	2FGL J1221.4+2814	W Com	bzb	LSP	M-11	10627	7027
F12248+8044	1FGL J1224.8+8044	2FGL J1223.9+8043	CRATES J1223+8040	bzb	ISP	N-06
J12248+4335	1FGL J1225.8+4336*	2FGL J1225.0+4335**	B3 1222+438	agu	LSP	fit	25354	7824
J12249+2122 ^M	1FGL J1224.7+2121	2FGL J1224.9+2122	4C +21.35	bzq	LSP	M-11	6612	40266
J12269+4340	1FGL J1225.8+4336*	2FGL J1225.0+4335**	B3 1224+439	bzq	ISP	fit	120486	33357
J12302+2518	1FGL J1230.4+2520	2FGL J1230.2+2517	ON 246	bzb	ISP	N-06	5782	4484
F12316+2850	1FGL J1231.6+2850	2FGL J1231.7+2848	B2 1229+29	bzb	HSP	2LAC	14203	12907
F12431+3627	1FGL J1243.1+3627	2FGL J1243.1+3627	B2 1240+36	bzb	HSP	M-11	26724	16535
J12483+5820 ^M	1FGL J1248.2+5820	2FGL J1248.2+5820	CGRaBS J1248+5820	bzb	HSP	N-06	41029	15463
J12531+5301	1FGL J1253.0+5301	2FGL J1253.1+5302	CRATES J1253+5301	bzb	ISP	N-06
J12579+3229	1FGL J1258.3+3227	2FGL J1258.2+3231	B2 1255+32	bzq	LSP	2LAC	4721	4833
J13030+2433 ^M	1FGL J1303.0+2433	2FGL J1303.1+2435	CRATES J1303+2433	bzb	LSP	fit	25134	13368
F13060+7852	1FGL J1306.0+7852	2FGL J1305.7+7854	CRATES J1305+7854	agu
J13083+3546	1FGL J1308.5+3550	2FGL J1308.5+3547	CGRaBS J1308+3546	bzq	LSP	2LAC	13335	5903
F13092+1156	1FGL J1309.2+1156	2FGL J1309.3+1154	4C +12.46	bzb	LSP	N-06
J13104+3220 ^M	1FGL J1310.6+3222	2FGL J1310.6+3222	B2 1308+32	bzq	LSP	M-11	10684	4824
J13127+4828	1FGL J1312.4+4827	2FGL J1312.8+4828	CGRaBS J1312+4828	bzq	LSP	2LAC	31078	75540
J13147+2348	1FGL J1314.7+2346	2FGL J1314.6+2348	CRATES J1314+2348	bzb	HSP	N-06
J13176+3425	1FGL J1317.8+3425	2FGL J1317.9+3426	B2 1315+34A	bzq	LSP	2LAC	8214	3038
J13211+2216	1FGL J1321.1+2214	...	CGRaBS J1321+2216	bzq	LSP	fit	11720	...
F13213+8310	1FGL J1321.3+8310	2FGL J1322.6+8313	CRATES J1321+8316	agu	13852	8286
J13270+2210	1FGL J1326.6+2213	2FGL J1326.8+2210	B2 1324+22	bzq	LSP	M-11	6870	6316
J13307+5202	1FGL J1331.0+5202	...	CGRaBS J1330+5202	agn	LSP	fit	24849	...
J13327+4722	1FGL J1332.9+4728	2FGL J1332.7+4725	B3 1330+476	bzq	LSP	2LAC	9111	5082
J13338+5057	1FGL J1333.2+5056	2FGL J1333.5+5058	CLASS J1333+5057	agu	LSP	2LAC	186614	79197
J13455+4452	1FGL J1345.4+4453	2FGL J1345.4+4453	B3 1343+451	bzq	LSP	2LAC	41634	34870
J13508+3034	1FGL J1351.0+3035	2FGL J1350.8+3035**	B2 1348+30B	bzq	LSP	2LAC	4955	5533
F13533+1434	1FGL J1353.3+1434	2FGL J1353.3+1435	PKS 1350+148	bzb	LSP	2LAC

Table 1—Continued

Source Name	1FGL Name	2FGL Name	Alternate AGN Name	Opt. Type	SED Type	SED Ref	$G_{r,1FGL}$	$G_{r,2FGL}$
F13581+7646	1FGL J1358.1+7646	2FGL J1358.1+7644	CGRaBS J1357+7643	bzq	LSP	2LAC	11881	5137
J13590+5544	1FGL J1359.1+5539	2FGL J1359.4+5541	CRATES J1359+5544	bzq	LSP	fit	42718	22483
J14270+2348 ^M	1FGL J1426.9+2347	2FGL J1427.0+2347	PKS 1424+240	bzb	HSP	N-06
J14340+4203	1FGL J1433.9+4204	2FGL J1433.8+4205	B3 1432+422	bzq	LSP	fit	20675	12034
J14366+2321	1FGL J1436.9+2314	2FGL J1436.9+2319	PKS 1434+235	bzq	LSP	2LAC	4730	6099
J14388+3710	1FGL J1438.7+3711*	2FGL J1438.7+3712**	B2 1436+37B	bzq	LSP	2LAC	24552	20208
F14387+3711	1FGL J1438.7+3711*	2FGL J1438.7+3712**	CRATES J1439+3712	bzq	LSP	2LAC	96541	81893
F14438+2457	1FGL J1443.8+2457	2FGL J1444.1+2500	PKS 1441+25	bzq	LSP	2LAC	6285	5206
J14509+5201	1FGL J1451.0+5204	...	CLASS J1450+5201	bzb
J14544+5124	1FGL J1454.6+5125	2FGL J1454.4+5123	CRATES J1454+5124	bzb	ISP	2LAC	59853	32796
F15044+1029 ^M	1FGL J1504.4+1029	2FGL J1504.3+1029	PKS 1502+106	bzq	LSP	M-11	150686	64921
J15061+3730	1FGL J1505.8+3725	2FGL J1506.0+3729	B2 1504+37	bzq	LSP	fit	4451	2347
J15169+1932 ^M	1FGL J1516.9+1928	2FGL J1516.9+1925	PKS 1514+197	bzb	LSP	M-11	5431	3624
F15197+4216	1FGL J1519.7+4216	2FGL J1520.9+4209	B3 1518+423	bzq	37320	20583
J15221+3144 ^M	1FGL J1522.1+3143	2FGL J1522.1+3144	B2 1520+31	bzq	LSP	2LAC	132237	95093
J15396+2744	1FGL J1539.7+2747	2FGL J1539.5+2747	CGRaBS J1539+2744	bzq	LSP	2LAC	12644	8504
J15429+6129 ^M	1FGL J1542.9+6129	2FGL J1542.9+6129	CRATES J1542+6129	bzb	ISP	M-11
F15534+1255 ^M	1FGL J1553.4+1255	2FGL J1553.5+1255	PKS 1551+130	bzq	LSP	fit	21961	7577
F15557+1111 ^M	1FGL J1555.7+1111	2FGL J1555.7+1111	PG 1553+113	bzb	HSP	N-06	22277	17485
J16046+5714	1FGL J1604.3+5710	2FGL J1604.6+5710	CGRaBS J1604+5714	bzq	LSP	2LAC	13645	10693
J16071+1551	1FGL J1607.1+1552	2FGL J1607.0+1552	4C +15.54	agn	LSP	M-11	6887	5501
F16090+1031	1FGL J1609.0+1031	2FGL J1608.5+1029	4C +10.45	bzq	LSP	M-11	8528	5523
J16136+3412 ^M	1FGL J1613.5+3411	2FGL J1613.4+3409	B2 1611+34	bzq	LSP	M-11	907	591
J16160+4632	1FGL J1616.1+4637	...	CRATES J1616+4632	bzq	LSP	fit	61224	...
F16302+5220	1FGL J1630.2+5220	2FGL J1630.4+5218	CRATES J1630+5221	bzb	ISP	2LAC
F16354+8228	1FGL J1635.4+8228	2FGL J1629.4+8236	NGC 6251	agn	LSP	M-11	2942	983
J16377+4717	1FGL J1637.9+4707	2FGL J1637.7+4714	4C +47.44	bzq	LSP	M-11	5891	5219
F16410+1143	1FGL J1641.0+1143	2FGL J1641.0+1141	CRATES J1640+1144	agn	17669	7987
J16475+4950	1FGL J1647.4+4948	2FGL J1647.5+4950	CGRaBS J1647+4950	agn	ISP	2LAC	8867	8153
J16568+6012	1FGL J1656.9+6017	2FGL J1656.5+6012	CRATES J1656+6012	bzq	LSP	2LAC	3957	3412
F17001+6830 ^M	1FGL J1700.1+6830	2FGL J1700.2+6831	CGRaBS J1700+6830	bzq	LSP	2LAC	8789	11526
J17096+4318	1FGL J1709.6+4320	2FGL J1709.7+4319	B3 1708+433	bzq	LSP	2LAC	31268	27091
F17192+1745 ^M	1FGL J1719.2+1745	2FGL J1719.3+1744	PKS 1717+177	bzb	LSP	M-11	3062	1129
F17225+1012	1FGL J1722.5+1012	2FGL J1722.7+1013	CRATES J1722+1013	bzq	LSP	2LAC	12070	7465
J17240+4004	1FGL J1724.0+4002	2FGL J1724.0+4003	B2 1722+40	agn	LSP	N-06	12010	9989
F17250+1151 ^M	1FGL J1725.0+1151	2FGL J1725.0+1151	CGRaBS J1725+1152	bzb	HSP	N-06	32112	27437
J17274+4530 ^M	1FGL J1727.3+4525	2FGL J1727.1+4531	B3 1726+455	bzq	LSP	M-11	3774	4284

Table 1—Continued

Source Name	1FGL Name	2FGL Name	Alternate AGN Name	Opt. Type	SED Type	SED Ref	$G_{r,1FGL}$	$G_{r,2FGL}$
J17283+5013	1FGL J1727.9+5010	2FGL J1728.2+5015	I Zw187	bzb	HSP	M-11	8874	4417
F17308+3716	1FGL J1730.8+3716	2FGL J1731.3+3718	CRATES J1730+3714	bzb	ISP	2LAC
J17343+3857 ^M	1FGL J1734.4+3859	2FGL J1734.3+3858	B2 1732+38A	bzq	LSP	2LAC	10666	5878
J17425+5945	1FGL J1742.1+5947	2FGL J1742.1+5948	CRATES J1742+5945	bzb	ISP	M-11
F17442+1934	1FGL J1744.2+1934	2FGL J1744.1+1934	1ES 1741+196	bzb	HSP	N-06	4098	2228
F17485+7004	1FGL J1748.5+7004	2FGL J1748.8+7006	CGRaBS J1748+7005	bzb	LSP	M-11	3660	2589
J17490+4321	1FGL J1749.0+4323	2FGL J1749.1+4323	B3 1747+433	bzb	LSP	M-11
F17566+5524	1FGL J1756.6+5524*	...	CRATES J1757+5523	agn	LSP	fit	28753	13989
F18004+7827 ^M	1FGL J1800.4+7827	2FGL J1800.5+7829	CGRaBS J1800+7828	bzb	LSP	M-11	2119	2160
F18070+6945 ^M	1FGL J1807.0+6945	2FGL J1806.7+6948	3C 371	bzb	ISP	M-11	2720	1674
F18096+2908	1FGL J1809.6+2908	2FGL J1809.7+2909	CRATES J1809+2910	bzb
F18134+3141	1FGL J1813.4+3141	2FGL J1813.5+3143	B2 1811+31	bzb	HSP	N-06	15967	10872
F18240+5651 ^M	1FGL J1824.0+5651	2FGL J1824.0+5650	4C +56.27	bzb	LSP	M-11	5013	4875
F18485+3224 ^M	1FGL J1848.5+3224	2FGL J1848.5+3216	B2 1846+32A	bzq	LSP	2LAC	21979	21036
F18493+6705 ^M	1FGL J1849.3+6705	2FGL J1849.4+6706	CGRaBS J1849+6705	bzq	LSP	A-11	13397	5139
F18525+4853	1FGL J1852.5+4853	2FGL J1852.5+4856	CGRaBS J1852+4855	bzq	LSP	2LAC	16991	11696
F19030+5539 ^M	1FGL J1903.0+5539	2FGL J1903.3+5539	CRATES J1903+5540	bzb	ISP	N-06
F19416+7214	1FGL J1941.6+7214	2FGL J1941.6+7218	CRATES J1941+7221	agu
F20000+6508 ^M	1FGL J2000.0+6508	2FGL J2000.0+6509	1ES 1959+650	bzb	HSP	N-06	14530	10334
F20019+7040	1FGL J2001.9+7040	2FGL J2001.7+7042	CRATES J2001+7040	agu	LSP	2LAC
F20060+7751	1FGL J2006.0+7751	2FGL J2004.5+7754	CGRaBS J2005+7752	bzb	LSP	M-11	3248	1172
F20091+7228	1FGL J2009.1+7228	2FGL J2009.7+7225	4C +72.28	bzb	LSP	N-06
F20204+7608	1FGL J2020.4+7608	2FGL J2022.5+7614	CGRaBS J2022+7611	bzb	ISP	N-06
F20315+1219 ^M	1FGL J2031.5+1219	2FGL J2031.7+1223	PKS 2029+121	bzb	LSP	2LAC	5603	2629
F20354+1100	1FGL J2035.4+1100	2FGL J2035.4+1058	PKS 2032+107	bzq	LSP	N-06	12343	7609
F20497+1003	1FGL J2049.7+1003*	2FGL J2049.8+1001	PKS 2047+098	agu
F21155+2937	1FGL J2115.5+2937	2FGL J2115.3+2932	B2 2113+29	bzq	LSP	2LAC	8184	4537
F21161+3338	1FGL J2116.1+3338	2FGL J2116.2+3339	B2 2114+33	bzb	ISP	2LAC
F21209+1901	1FGL J2120.9+1901	2FGL J2121.0+1901	OX 131	bzq	LSP	2LAC	20415	14131
F21434+1742 ^M	1FGL J2143.4+1742	2FGL J2143.5+1743	OX 169	bzq	LSP	M-11	13782	10365
F21525+1734	1FGL J2152.5+1734	2FGL J2152.4+1735	PKS 2149+17	bzb	LSP	N-06	3435	3951
F21574+3129	1FGL J2157.4+3129	2FGL J2157.4+3129	B2 2155+31	bzq	LSP	2LAC	17937	16558
F22035+1726 ^M	1FGL J2203.5+1726	2FGL J2203.4+1726	PKS 2201+171	bzq	LSP	M-11	15029	10498
F22121+2358	1FGL J2212.1+2358	2FGL J2211.9+2355	PKS 2209+236	bzq	LSP	2LAC	2230	1340
F22171+2423	1FGL J2217.1+2423	2FGL J2217.1+2422	B2 2214+24B	bzb	LSP	2LAC	5967	3161
F22193+1804	1FGL J2219.3+1804	2FGL J2219.1+1805	CGRaBS J2219+1806	bzq	20104	7251
F22362+2828 ^M	1FGL J2236.2+2828	2FGL J2236.4+2828	B2 2234+28A	bzq	LSP	M-11	5173	2914

Table 1—Continued

Source Name	1FGL Name	2FGL Name	Alternate AGN Name	Opt. Type	SED Type	SED Ref	$G_{r,1FGL}$	$G_{r,2FGL}$
F22440+2021 ^M	1FGL J2244.0+2021	2FGL J2243.9+2021	CRATES J2243+2021	bzb	HSP	2LAC
F22501+3825	1FGL J2250.1+3825	2FGL J2250.0+3825	B3 2247+381	bzb	HSP	N-06	18920	13435
F22517+4030	1FGL J2251.7+4030	2FGL J2251.9+4032	CRATES J2251+4030	bzb
F22539+1608 ^M	1FGL J2253.9+1608	2FGL J2253.9+1609	3C 454.3	bzq	LSP	M-11	12137	15731
F23073+1452	1FGL J2307.3+1452	2FGL J2308.0+1457	CGRaBS J2307+1450	bzb	LSP	fit	30212	40301
F23110+3425	1FGL J2311.0+3425	2FGL J2311.0+3425	B2 2308+34	bzq	LSP	2LAC	12526	12080
F23220+3208	1FGL J2322.0+3208	2FGL J2322.2+3206	B2 2319+31	bzq	LSP	2LAC	10989	4821
F23216+2726	1FGL J2321.6+2726	2FGL J2321.0+2737	4C +27.50	bzq	LSP	2LAC	5914	2546
F23226+3435	1FGL J2322.6+3435	2FGL J2322.6+3435	CRATES J2322+3436	bzb	HSP	N-06	52497	13883
F23252+3957	1FGL J2325.2+3957	2FGL J2325.3+3957	B3 2322+396	bzb	HSP	N-06

Note. — Col. (1): Source Name: if name starts with 'J' it is a VIPS or pre-1FGL MOJAVE source; if name starts with 'F' it is a source targeted specifically for its presence in 1FGL. Col. (2): 1FGL source name. Col. (3): 2FGL source name. Col. (4): Other AGN name. Col. (5): Optical Type from 2LAC/1LAC: bzb = BL Lac object, bzq = FSRQ, agn = non-blazar AGN, agu = AGN of uncertain type, sbg = starburst galaxy. Col. (6): SED type: LSP=low-synchrotron peaked, ISP=intermediate-synchrotron peaked, HSP=high-synchrotron peaked. Col. (7): Reference for SED type: 0FGL = Abdo et al. 2010c, N-06 = Nieppola et al. 2006, N-08 = Nieppola et al. 2008, A-11 = Aatrokoski et al. 2011, M-11 = Meyer et al. 2011, 2LAC = estimated using technique in Ackermann et al. 2011, fit = log-parabolic fit to NED data. Col. (8): Gamma-ray loudness using 1FGL data. Col. (9): Gamma-ray loudness using 2FGL data.

^MMOJAVE source that was included in Lister et al. (2011). For more data, visit the MOJAVE website <http://www.physics.purdue.edu/astro/MOJAVE/MOJAVEItable.html> or see Lister et al. (2009b, 2011)

*Indicates a LAT source which is associated with multiple radio sources with high ($\geq 80\%$) probability in 1LAC

**Indicates a LAT source which is associated with multiple radio sources with high ($\geq 80\%$) probability in 2LAC

^cIndicates a 2FGL source that is considered to be potentially confused with galactic diffuse emission

Table 2. BL Lac Object $G_r - \nu_{peak}^S$ Correlations

LAT data	BL Lac Sample	Spearman ρ_S	Spearman p
1FGL	Original BL Lac Object Sample (27 LBLs)	0.46	0.0003
	Adding 7 LSP FSRQs	0.42	0.0005
	Adding 14 LSP FSRQs	0.37	0.001
	Adding 27 LSP FSRQs	0.30	0.005
	Adding 54 LSP FSRQs	0.17	0.07
	Adding all 96 LSP FSRQs	0.14	0.08
2FGL	Original BL Lac Object Sample (26 LBLs)	0.40	0.003
	Adding 7 LSP FSRQs	0.30	0.02
	Adding 13 LSP FSRQs	0.30	0.01
	Adding 26 LSP FSRQs	0.25	0.02
	Adding 52 LSP FSRQs	0.13	0.2
	Adding all 91 LSP FSRQs	0.12	0.2

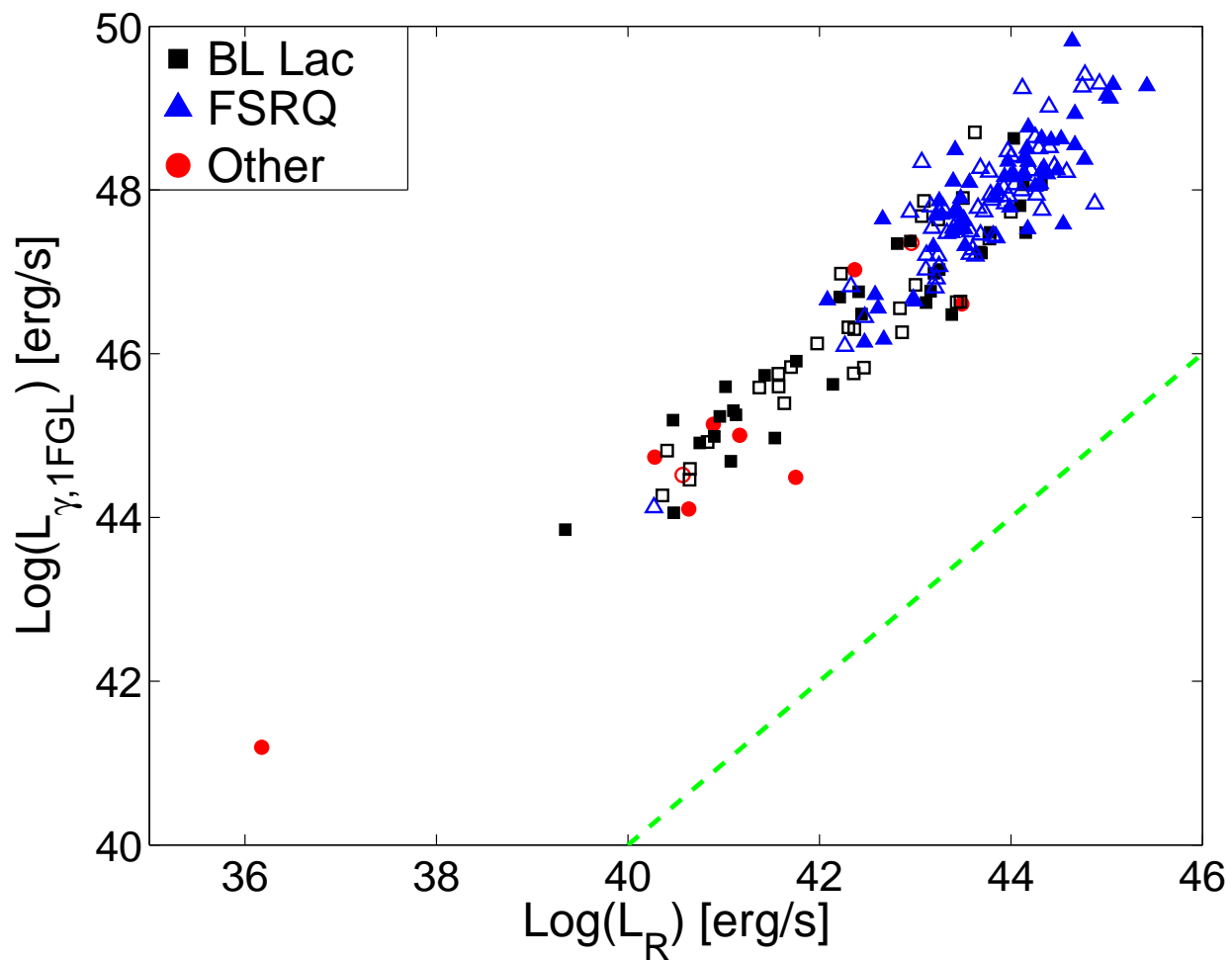


Fig. 1.— 1FGL γ -ray luminosity versus total VLBA luminosity at 5 GHz. Black squares indicate BL Lac objects, blue triangles are FSRQs, and red circles are AGN/other. Unfilled symbols are used for sources in VIPS+ and filled symbols are used for sources in VIPS++ (see Section 2). The dashed green line indicates a 1:1 luminosity ratio; any source above this line is considered γ -ray loud. The “other”-type source in the lower left is the starburst galaxy M82. The 2FGL luminosity-luminosity plot is very similar.

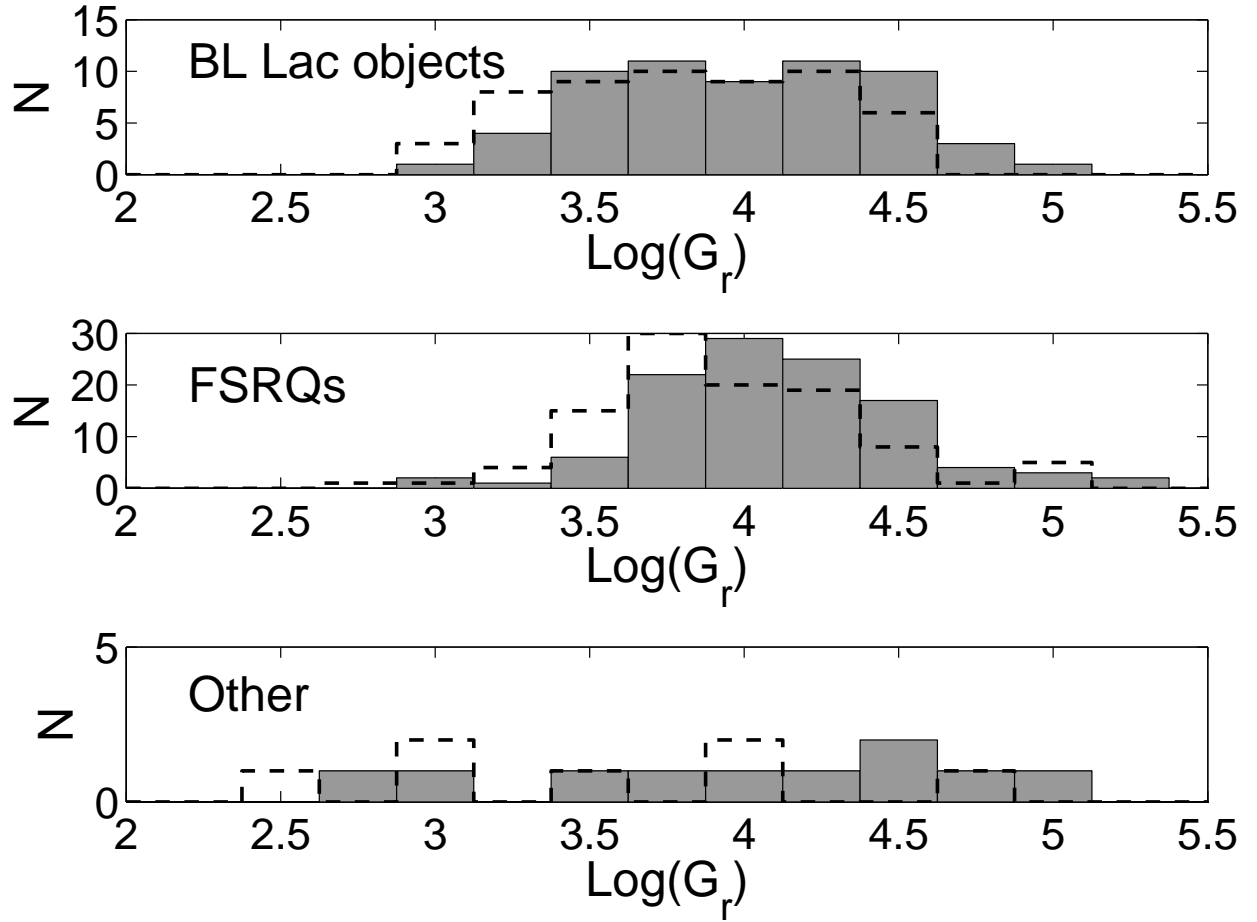


Fig. 2.— Distributions of γ -ray to radio luminosity ratio for BL Lac objects (top), FSRQs (middle), and AGN/other (bottom). The gray bars are for 1FGL data and the dashed lines are for 2FGL data.

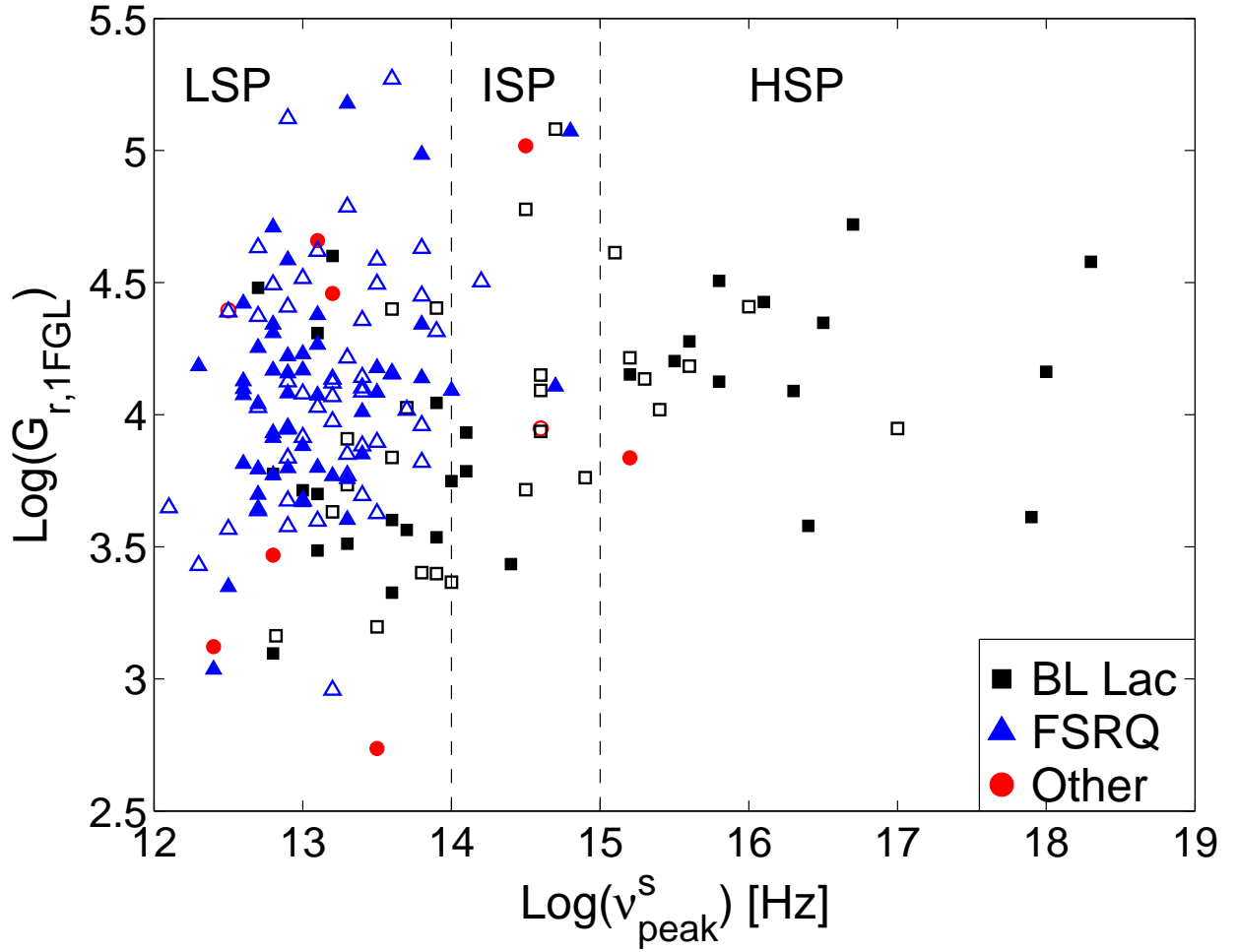


Fig. 3.— 1FGL γ -ray to radio luminosity ratio versus synchrotron peak frequency. Unfilled symbols are used for sources in VIPS+ and filled symbols are used for sources in VIPS++ (see Section 2). The dashed lines indicate the divisions between low-, intermediate-, and high-synchrotron peaked objects. The LSP “other”-type object with low G_r is the radio galaxy NGC 1275. The ISP “other”-type object with the relatively high G_r is the starburst galaxy M82. The plot for $G_{r,2FGL}$ versus ν_{peak}^S is very similar.

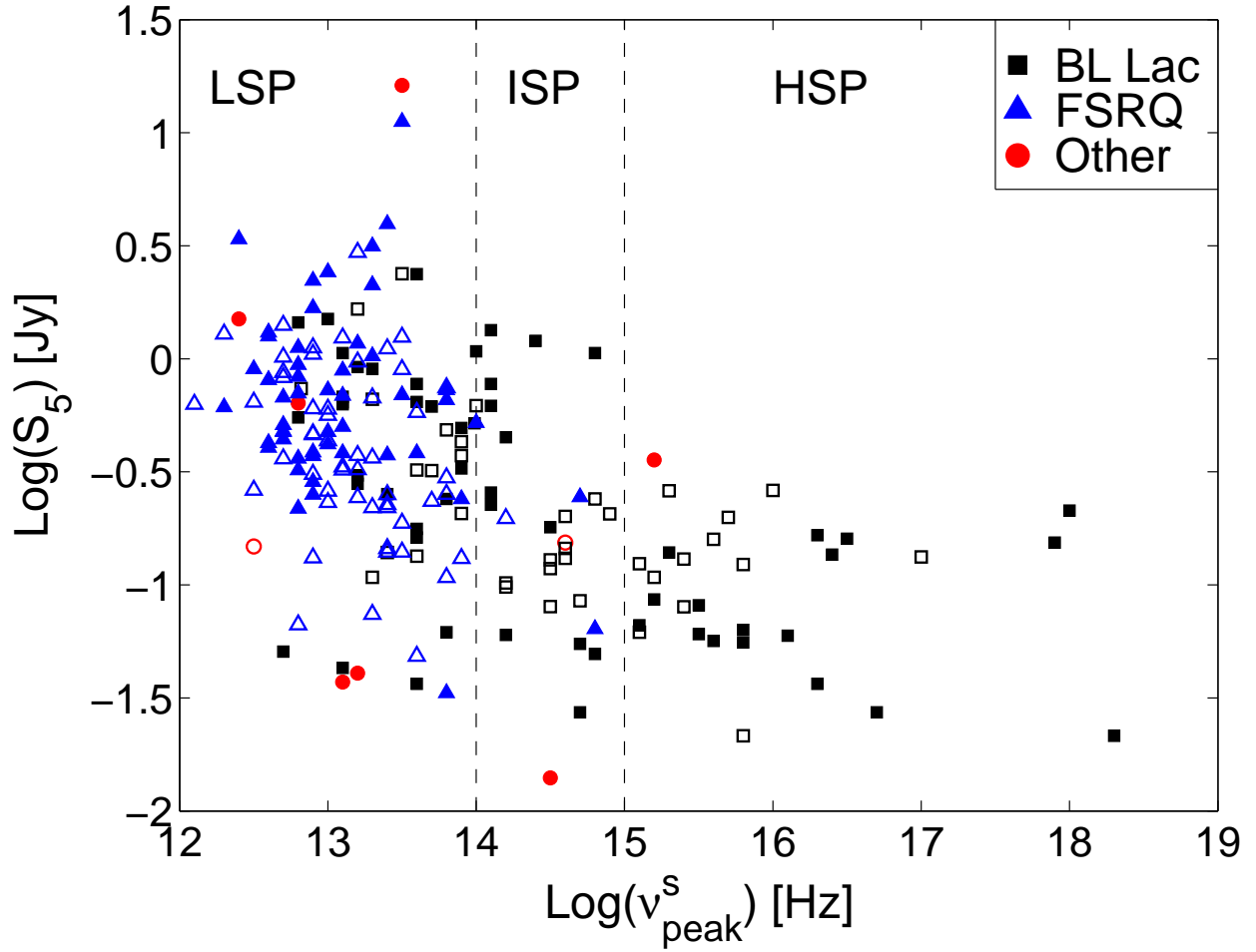


Fig. 4.— Total VLBA flux density at 5 GHz versus synchrotron peak frequency. Unfilled symbols are used for sources in VIPS+ and filled symbols are used for sources in VIPS++ (see Section 2). The dashed lines indicate the divisions between low-, intermediate-, and high-synchrotron peaked objects. The LSP “other”-type object with the high flux density is the radio galaxy NGC 1275. The ISP “other”-type object with the low flux density is the starburst galaxy M82.

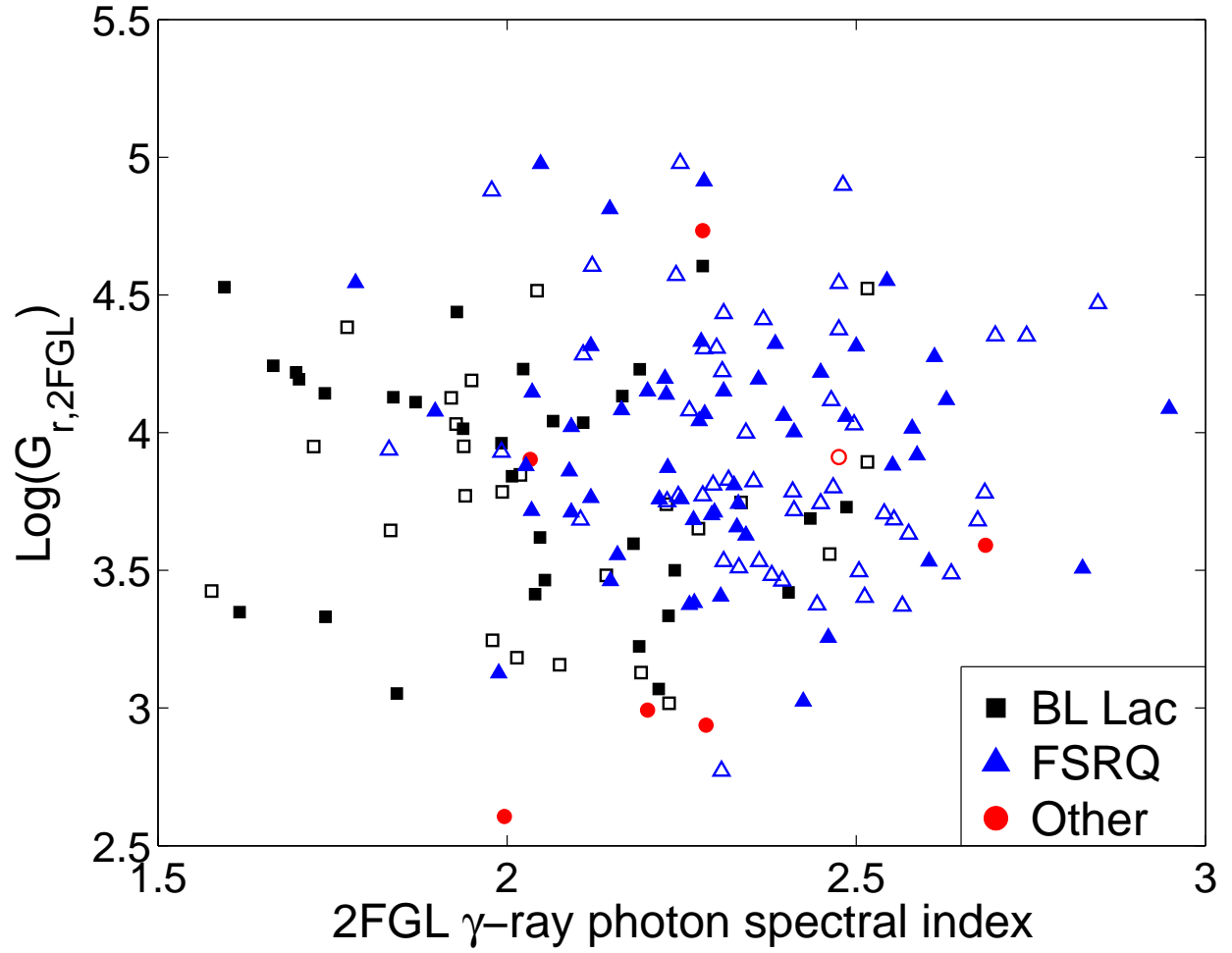


Fig. 5.— γ -ray loudness versus γ -ray photon spectral index (all data from 2FGL). Unfilled symbols are used for sources in VIPS+ and filled symbols are used for sources in VIPS++ (see Section 2). The “other”-type object with low G_r and a photon spectral index of about 2 is the radio galaxy NGC 1275.

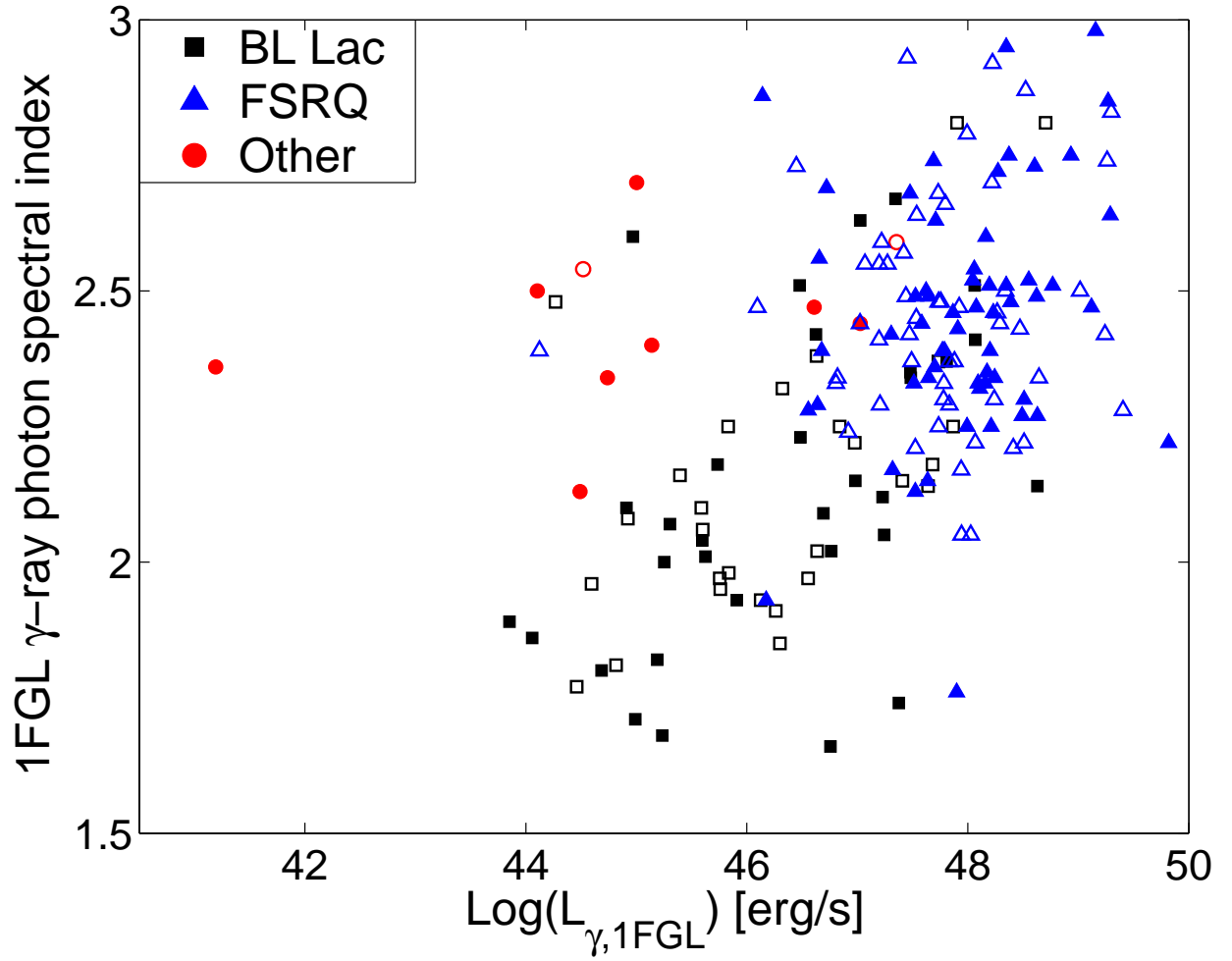


Fig. 6.— γ -ray photon spectral index versus γ -ray luminosity (all data from 1FGL). Unfilled symbols are used for sources in VIPS+ and filled symbols are used for sources in VIPS++ (see Section 2). The “other”-type object on the extreme left is the starburst galaxy M82.

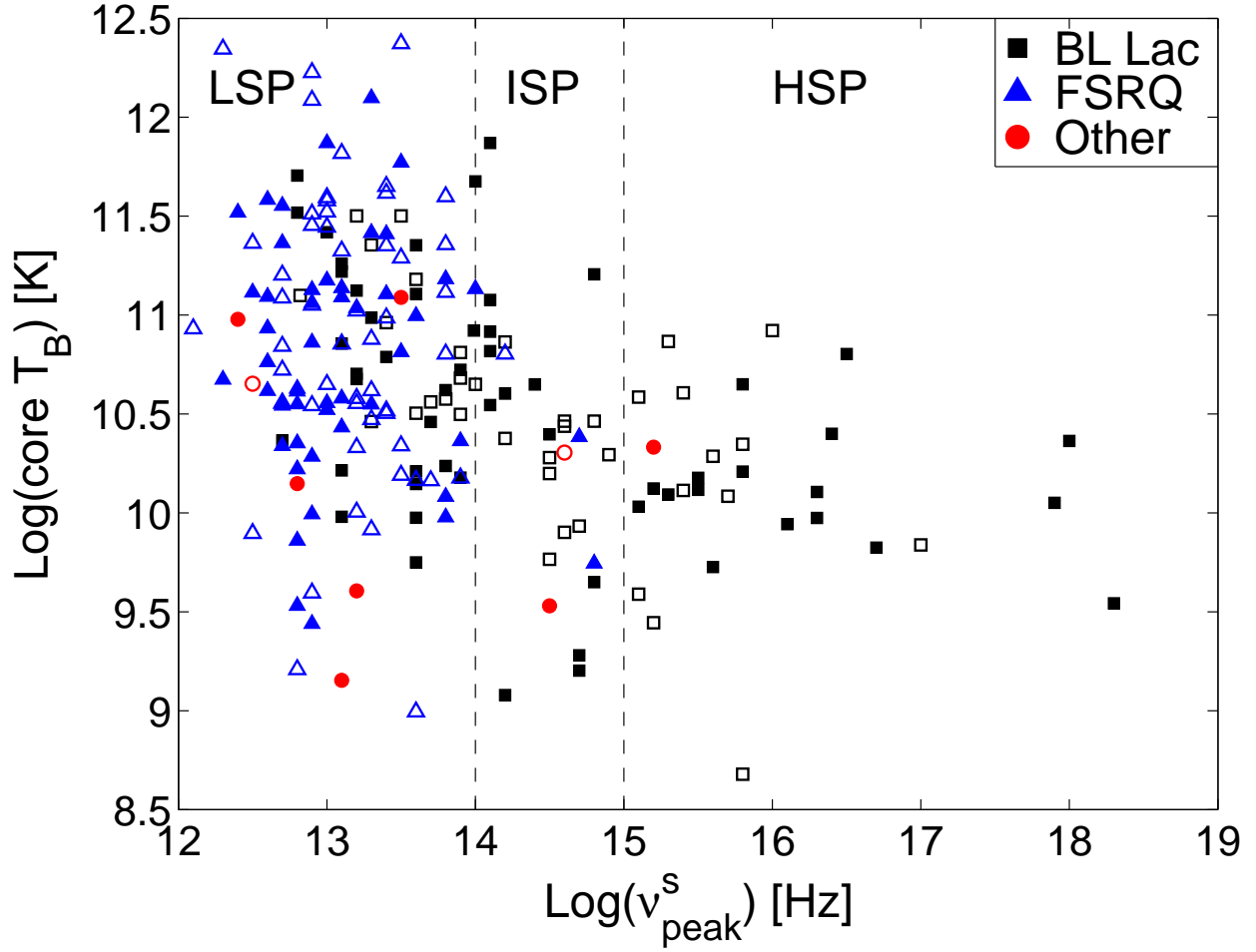


Fig. 7.— Core brightness temperature versus synchrotron peak frequency. Unfilled symbols are used for sources in VIPS+ and filled symbols are used for sources in VIPS++ (see Section 2). The dashed lines indicate the divisions between low-, intermediate-, and high-synchrotron peaked objects. The “other”-type object with the highest core T_B is the radio galaxy NGC 1275 (located in the LSP area). The starburst galaxy M82 is the ISP “other”-type object with the lower core T_B .

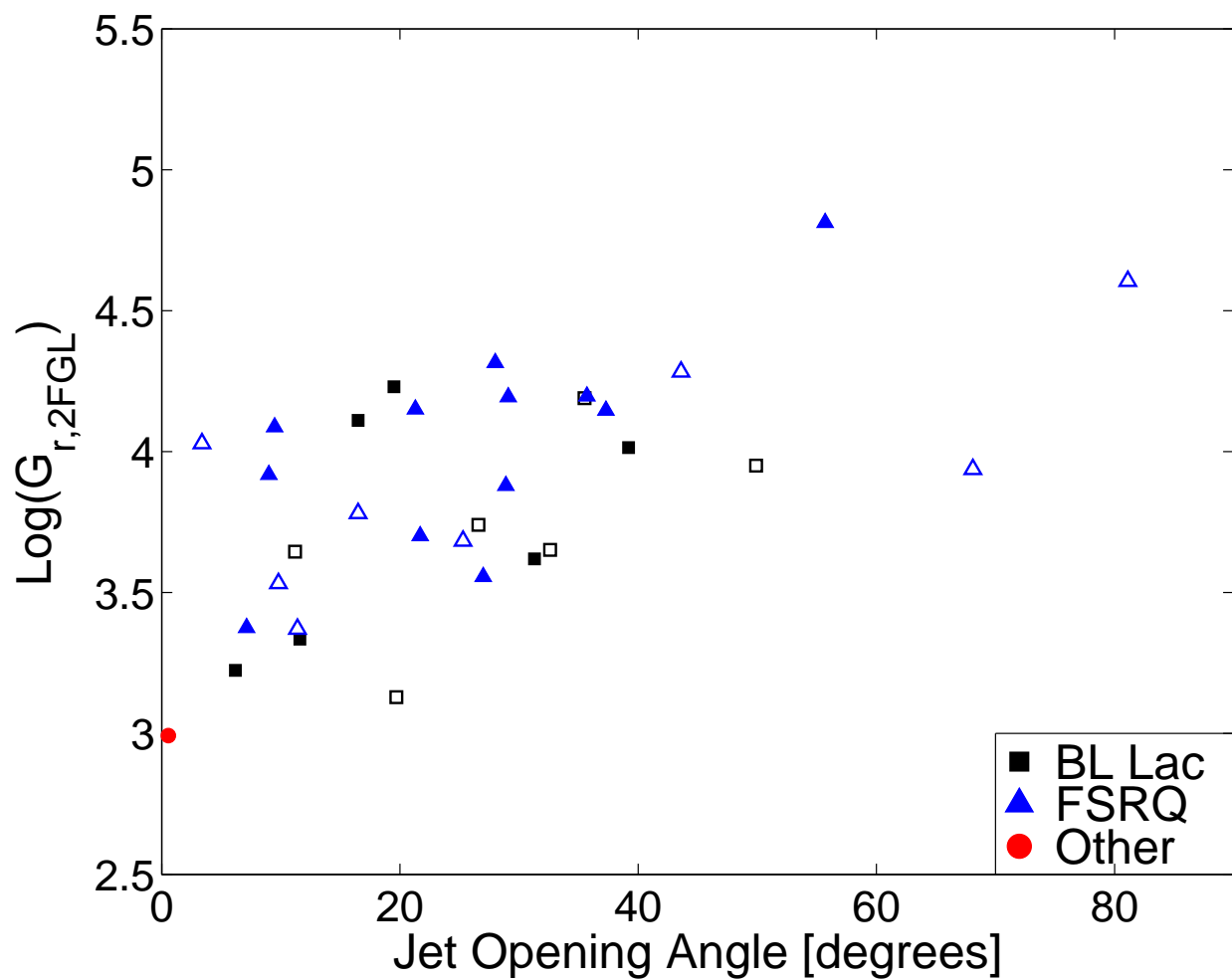


Fig. 8.— 2FGL γ -ray to radio luminosity ratio versus apparent jet opening angle. Unfilled symbols are used for sources in VIPS+ and filled symbols are used for sources in VIPS++ (see Section 2). The lone “other”-type object is the radio galaxy NGC 6251. The 1FGL data did not show a correlation.

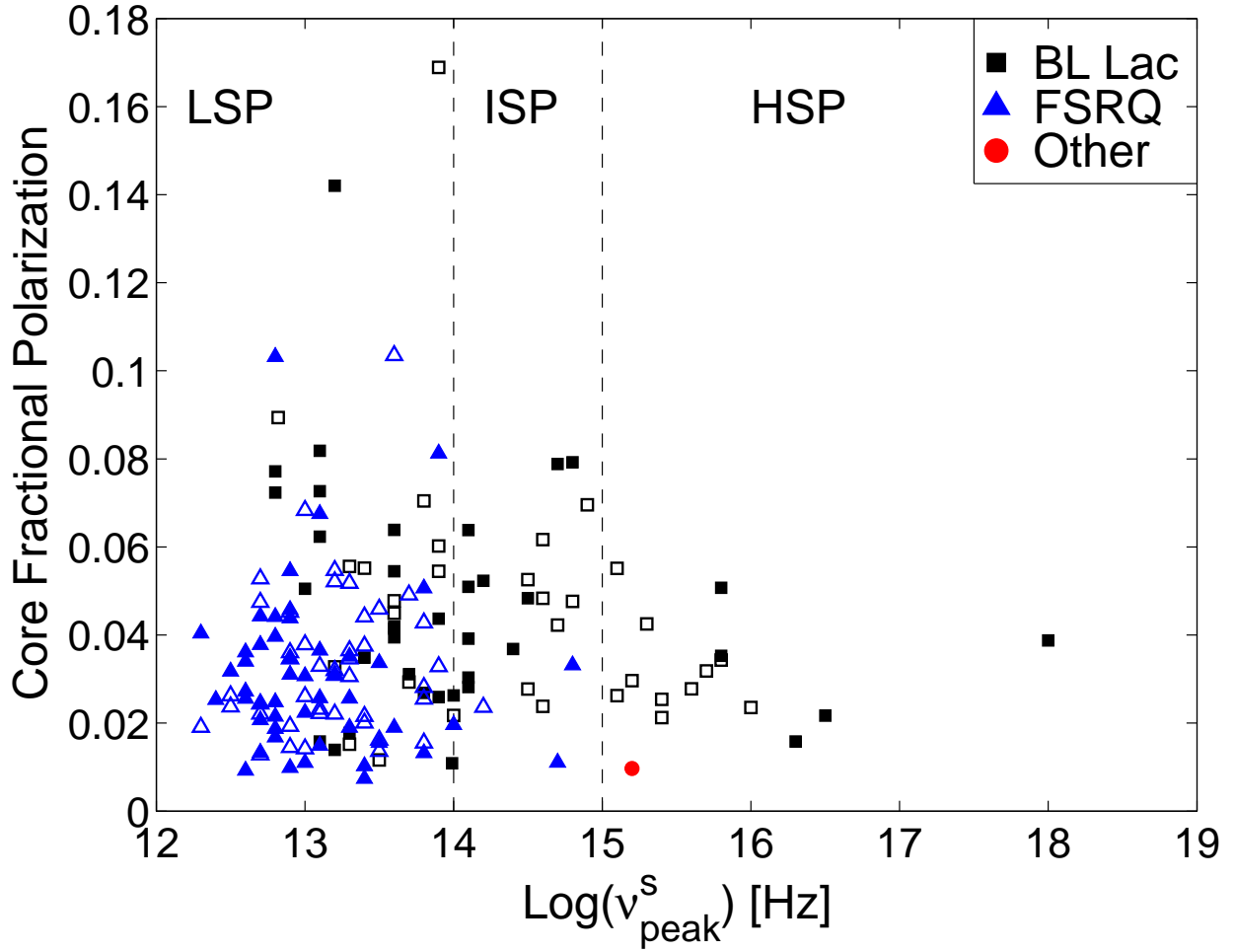


Fig. 9.— 5 GHz core fractional polarization versus synchrotron peak frequency. Unfilled symbols are used for sources in VIPS+ and filled symbols are used for sources in VIPS++ (see Section 2). The dashed lines indicate the divisions between low-, intermediate-, and high-synchrotron peaked objects. The lone “other”-type object is the source F03250+3403, which has an uncertain classification: NED lists it as a Seyfert 1, 1LAC called it a non-blazar AGN, and 2LAC listed its type as “unidentified”.

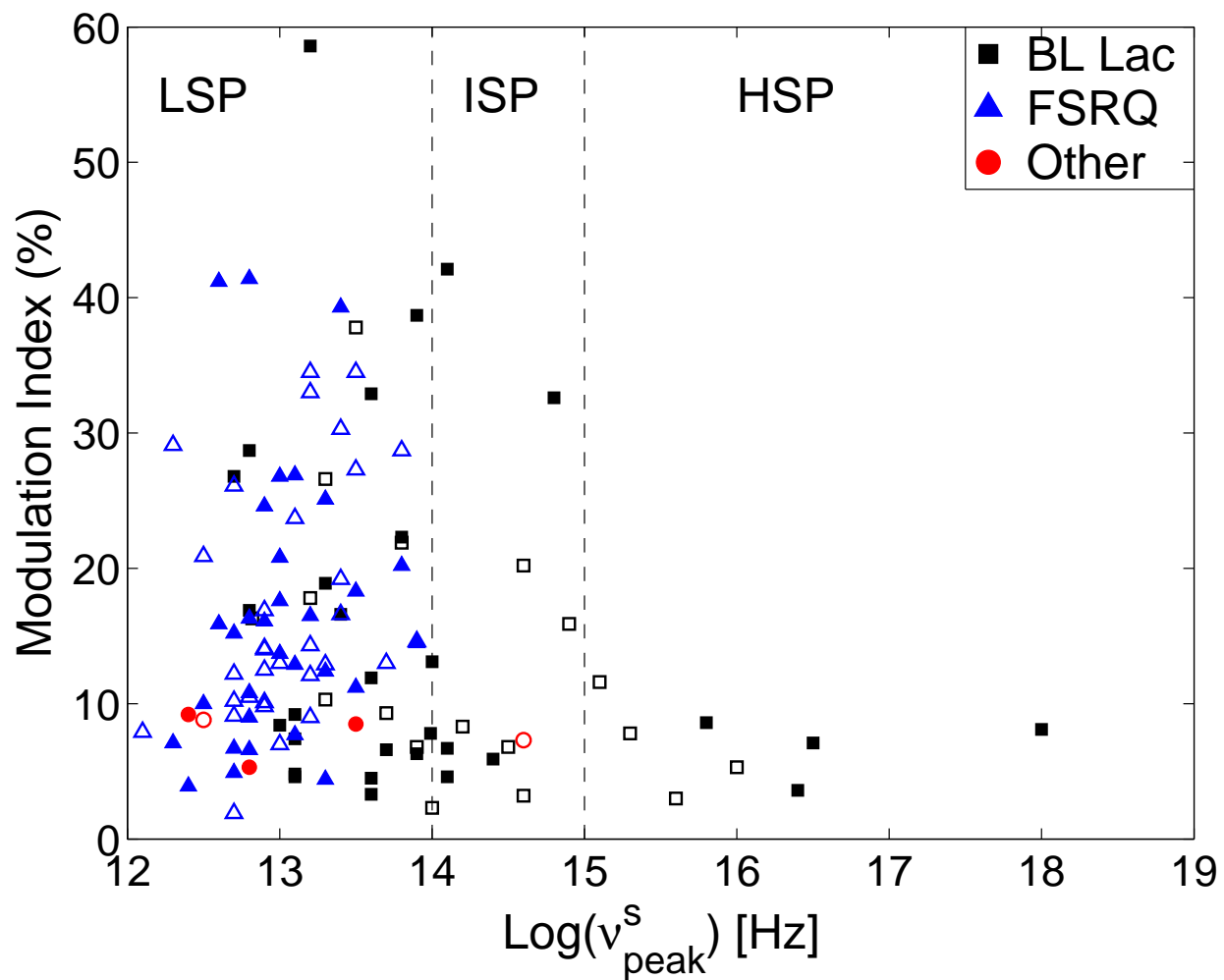


Fig. 10.— Modulation index from Richards et al. (2011) versus synchrotron peak frequency. Unfilled symbols are used for sources in VIPS+ and filled symbols are used for sources in VIPS++ (see Section 2). The dashed lines indicate the divisions between low-, intermediate-, and high-synchrotron peaked objects. The radio galaxies NGC 6251 and NGC 1275 are the LSP “other”-type sources with ν_{peak}^s values near 12.8 and 13.5, respectively.

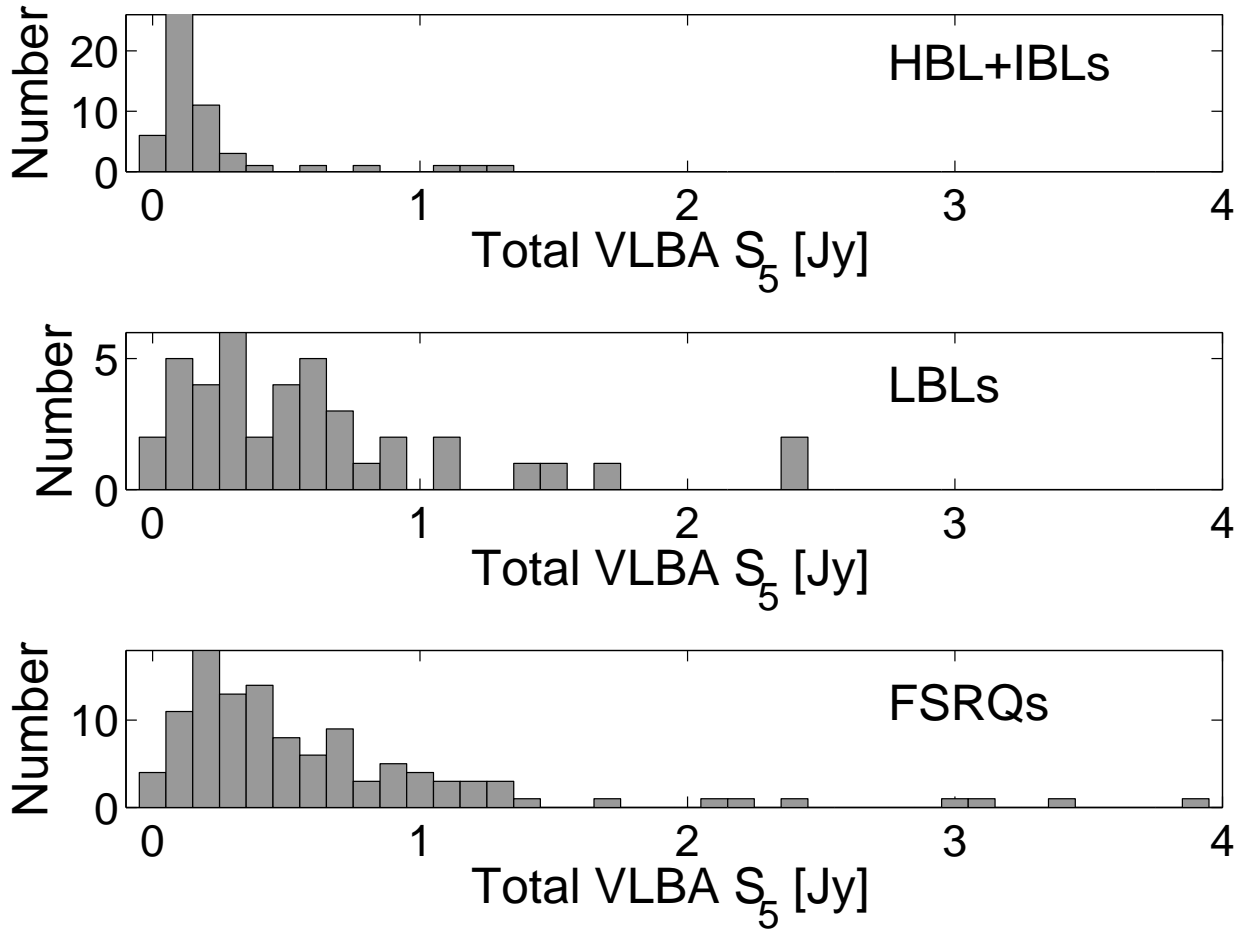


Fig. 11.— Distributions of total VLBA flux density at 5GHz for the combined HSP and ISP BL Lac objects (top), LSP BL Lac objects (middle), and FSRQs (bottom). We have omitted one FSRQ with a flux density of 11.2 Jy.

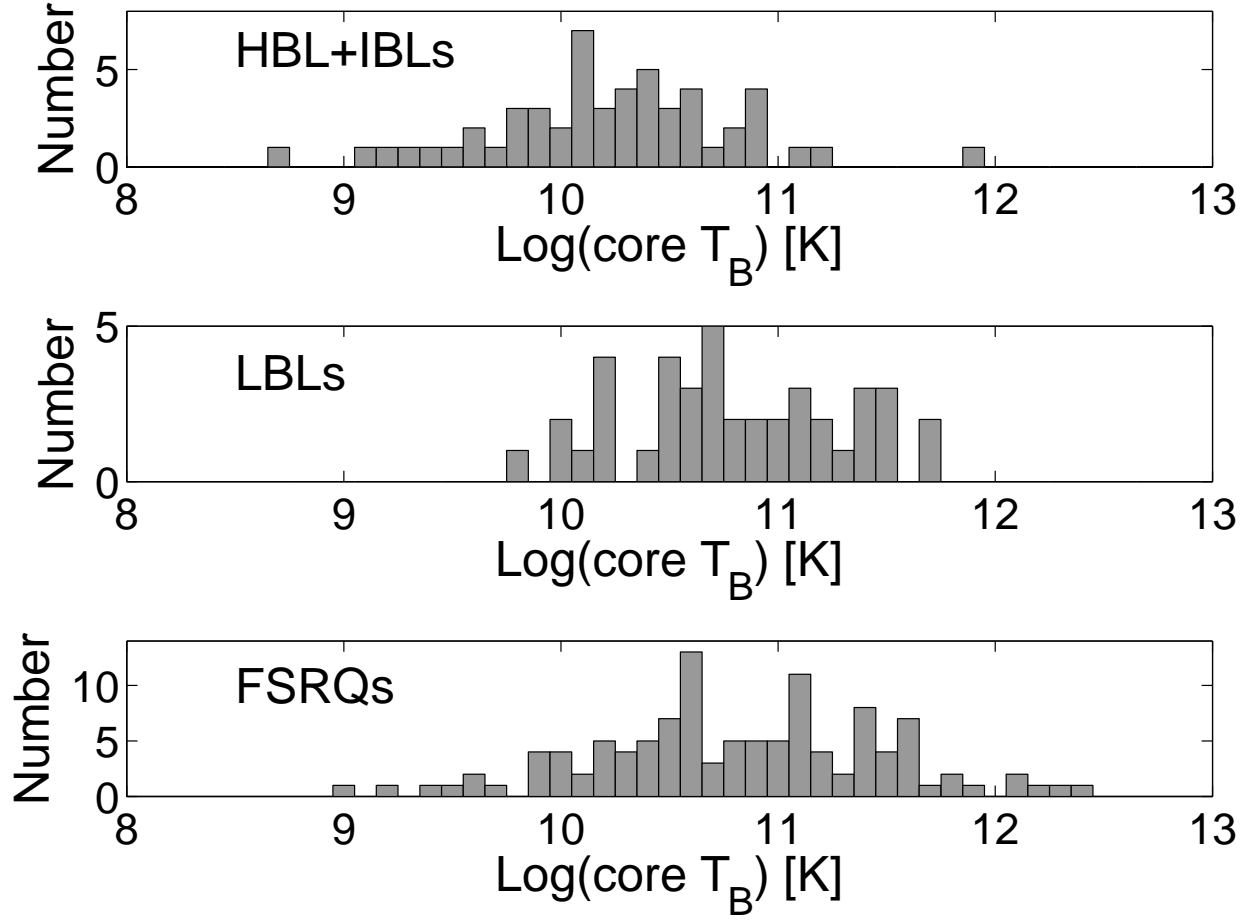


Fig. 12.— Distributions of core brightness temperatures for the combined HSP and ISP BL Lac objects (top), LSP BL Lac objects (middle), and FSRQs (bottom).